

4-Acyl Pyrroles as Dual BET-BRD7/9 Bromodomain Inhibitors Address BETi Insensitive Human Cancer Cell Lines

Martin Hügler, Pierre Regenass, Robin Warstat, Mirjam Hau, Karin Schmidtkunz, Xavier Lucas, Daniel Wohlwend, Oliver Einsle, Manfred Jung, Bernhard Breit, and Stefan Günther*

Cite This: <https://dx.doi.org/10.1021/acs.jmedchem.0c00478>

Read Online

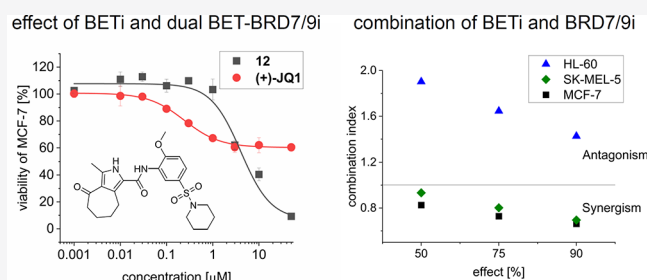
ACCESS |

Metrics & More

Article Recommendations

Supporting Information

ABSTRACT: Various malignant human diseases show disturbed signaling pathways due to increased activity of proteins within the epigenetic machinery. Recently, various novel inhibitors for epigenetic regulation have been introduced which promise a great therapeutic benefit. Inhibitors for the bromo- and extra-terminal domain (BET) family were of particular interest after inhibitors had shown a strong antiproliferative effect. More recently, the focus has increasingly shifted to bromodomains (BDs) outside the BET family. Based on previously developed inhibitors, we have optimized a small series of 4-acyl pyrroles, which we further analyzed by ITC, X-ray crystallography, selectivity studies, the NCI60 cell-panel, and GI₅₀ determinations for several cancer cell lines. The inhibitors address both, BET and BRD7/9 BDs, with very high affinity and show a strong antiproliferative effect on various cancer cell lines that could not be observed for BD family selective inhibitors. Furthermore, a synergistic effect on breast cancer (MCF-7) and melanoma (SK-MEL-5) was proven.



1. INTRODUCTION

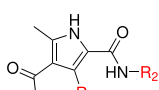
Epigenetic modifications, including but not limited to DNA methylation, histone composition, and post-translational modifications, control the behavior of a cell by regulating protein–DNA interactions.¹ While in healthy cells, these mechanisms control cell differentiation or chromatin maintenance, a malfunction can lead to serious diseases.² In this context, histone acetylations have been investigated as an epigenetic hallmark, and various interacting proteins were identified as potential drug targets. In recent years, the reader domains for acetylated lysines on histones, bromodomains (BDs), have increasingly moved to the foreground. The human genome comprises a total of 61 BDs in 46 BD-containing proteins. Although the BD sequences differ considerably in some cases, they all have a highly conserved overall fold. BDs comprise roughly 120 amino acids, which form a bundle of four left-handed α -helices, called α Z, α A, α B, and α C. The helices are connected by a short turn and two loops, called ZA and BC loops, which can differ substantially in length and sequence. The binding pocket is essential for the differentiation between unmodified and acetylated lysine (KAc). A highly conserved asparagine, rarely a threonine, tyrosine, or aspartate, serves to bind the KAc.³ The given selectivity of individual BDs for certain histone tails is primarily determined by interactions of the BD surface at the rim of the KAc binding site. However, additional epigenetic modifications of the histone tails can further modify the recognition by BDs.^{4,5} The best investigated BDs to date belong to the BET family. These are the BDs of the proteins

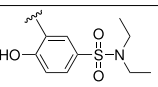
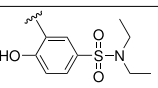
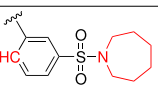
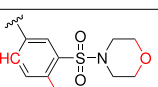
BRD2, BRD3, BRD4, and BRDT, each of them with two BDs and an extra-terminal domain. Already in 1990, two years before the discovery of the BDs, the first patent for a cancer and inflammation drug was granted, which addresses the BET family.⁶ In 2001, Marmorstein and Berger postulated a link between BDs, their ability to bind KAc and chromatin structural changes, as well as gene regulation.⁷ Despite these findings, it was only in 2010, with the success of the BET-BD inhibitors (+)-JQ1 and I-BET 762, that the importance and potential of this class of drugs was revealed.^{8,9} Since then, findings related to BDs and inhibitors have increased continuously. The most intensively investigated representative here is the BET family member BD-containing protein 4 (BRD4), in particular its first BD, BRD4(1).^{5,8–10} For example, a connection between cancer progression or inflammation and BRD4 could be proven,^{2,11,12} and several BRD4(1) inhibitors could be identified which demonstrated an antiproliferative effect on various cancer cell lines, such as (+)-JQ1, the I-BET series, or the XD series.^{13,14} BET inhibitors generally demonstrate a strong cytostatic effect but no apoptotic effect.¹⁵ Interestingly, first BET-BD inhibition-resistant cancer cell lines have been reported recently.¹⁶

Received: March 21, 2020

Various BET-BD inhibitors are currently in clinical or preclinical phases.^{17,18} However, the results are extremely heterogeneous, and many patients have exhibited therapy-resistant cancer types.¹⁵ Not least because of this, combination therapies were tested *in vivo* and showed that resistance could be circumvented or cytotoxicity in cancer cells could be established.¹⁵ However, the underlying mechanisms are only partially understood, which has already led to critical questioning regarding the early starts of clinical trials.¹⁹ Nevertheless, the overwhelming success of the BET-BD inhibitors also led to a more intensive investigation of other BDs and to the development of specific non-BET-BD inhibitors.¹⁸ For example, we recently demonstrated the refinement of the non-selective fragment **1** (Table 1) toward a

Table 1. ITC and Thermal Shift Assay^a Results for Previously Described Modification of **2**



#	R ₁	R ₂	$K_{D, BRD4(1)}$ [μ M]	ΔT_m [K]
1	Et	Me	16 ^[14]	n.d.
2	Et		0.24 ^[13]	+6.7 ^[14]
3	Me		0.51 ^[14]	+2.1 ^[14]
4	Pr		n.d.	+5.3 ^[14]
5	Et		1.3 ^[14]	+2.8 ^[14]

^a ΔT_m values represent the difference in thermal stability of BRD4(1) (20 μ M) with and without ligand (200 μ M). ΔT_m correlates with affinity, with higher ΔT_m values representing better affinity.

selective and active p300/CBP-BD inhibitor.²⁰ Other groups have developed inhibitors for the two closely related BDs of BRD7 and BRD9.^{21,22} Similarly, a selective BRD9-BD inhibitor has been developed with I-BRD9, which is selective even against BRD7.²³ First investigations with BRD7/BRD9-BD inhibitors have shown their potential as active agents for the prevention of epigenetically defined drug resistance or treatment of acute myeloid leukemia (AML).²⁴ Engineered resistant cells have validated the connection of BRD9 with AML.²⁵ The antitumor activity of a BRD7/BRD9-BD inhibitor was also shown in an AML xenograft model by the SGC and Boehringer Ingelheim.²¹ Furthermore, synergy of BRD9 and BET inhibition on triple negative breast cancer, as well as an underlying mechanism was found.²⁶

Originally designed as BET inhibitors, some derivatives of **2**^{13,14} (Table 1) showed differing binding profiles to various other BDs. In the study presented here, we set out to optimize the moderately active inhibitor **2** with respect to affinity and activity. The resulting inhibitors address both the BET family and BRD7/BRD9 with nanomolar K_D s and are significantly superior to (+)-JQ1 with respect to their efficacy on several

cancer cell lines, such as MCF-7 (breast cancer) and SK-MEL-5 (melanoma).

2. RESULTS

In the present study, applying previously obtained knowledge about derivatives¹⁴ of **2** (original name XD14),¹³ new modifications of **2** were designed and synthesized. We focused on optimizations of 4-acyl pyrrole (head), the hydroxyl group, and the *N,N*-diethyl sulfonamide (tail, Figure 1). Compounds were tested by means of isothermal titration calorimetry (ITC) and bromoscans. In addition, structures of all 8 new derivatives (**6**–**13**) complexed with BRD4(1) were investigated by means of X-ray crystallography to allow for further optimization. Changes in potency were assessed using the NCI60 panel and accompanied by more detailed analyses in the cell lines HL-60, MCF-7, and SK-MEL-5. Finally, a negative control for one of the most potent inhibitors was synthesized.

2.1. Optimization of the Head Group. The first step in this process was to optimize the head group (Figure 1). Initially, **1** (original name XD46), a mostly unspecific fragment of **2**,¹³ was optimized with respect to the affinity for BRD4(1). As we could already see in a previous study¹⁴ (Table 1), the 3-methylpyrrole derivative **3** (original name XD27) shows a lower affinity for BRD4(1) than the 3-ethylpyrrole derivative (**2**). The 3-propylpyrrole derivative **4** (original name XD42) features further modifications but suffers from a solubility too poor for ITC. However, in a previous study, we estimated a strong binding based on a thermal shift assay (TSA) (Table 1) as well as on the very well defined ligand in the crystal structure.¹⁴ Hence, we assumed that extending the hydrophobic 3-propyl pyrrole while maintaining the better solubility of **1** would have a positive effect on both solubility and target affinity as compared to **1**. In order to reduce the number of freely rotatable bonds, while further supporting hydrophobic interactions, compound **6** was generated by ring closure between the 4-acyl and the 3-alkyl of **1** (Figure 1). The structure of BRD4(1) in complex with **6** (Figure 2A) shows interactions as previously described for other 4-acyl pyrroles.^{13,14} In addition to hydrophobic interactions with Phe83, Val87, Leu94, Tyr139, and Ile146, the main interactions are the hydrogen bonds of 4-acyl to the conserved Asn140 and, through a bridging water to Tyr97, as well as a hydrogen bond of the pyrrole to the carbonyl backbone of Pro82. A direct structural comparison between **1** and **6** (Figure 3A) reveals a largely conserved binding mode. In both cases, the position of the amide linker is not fully covered by electron density, whereas the seven-membered ring of **6** is fully resolved in electron density. Apart from the CH₂ group newly inserted for the ring closure and the associated increased surface complementarity, the seven-membered ring shows no substantial changes compared to the corresponding 4-acyl and 3-alkyl moieties of **1**. In comparison to **4** (Figure 3B), however, there is a slight deviation in the positioning of the 4-acyl and 3-alkyl moiety.

2.2. Fragment Linking. As **6** showed a similar positioning as other 4-acyl pyrroles with BRD4(1), fragment **6** was linked to the tail of **2** to yield compound **7** (Figure 1 and Table 2). The crystal structure of **7** in complex with BRD4(1) verifies the expected binding mode. The head binds as seen for **6** and the tail very similar to **2**¹³ (Figure 3 C and D). The amide linker forms a hydrogen bond to a water coordinated by Glu85, while the aryl moiety addresses the WL-trap between Trp81 and Leu92. The sulfonamide is comparably oriented as for **2**. With ITC, it was validated that this binding mode produces a significant gain in affinity to BRD4(1) ($K_{D, BRD4(1)} = 72$ nM, Tables 2 and 3)

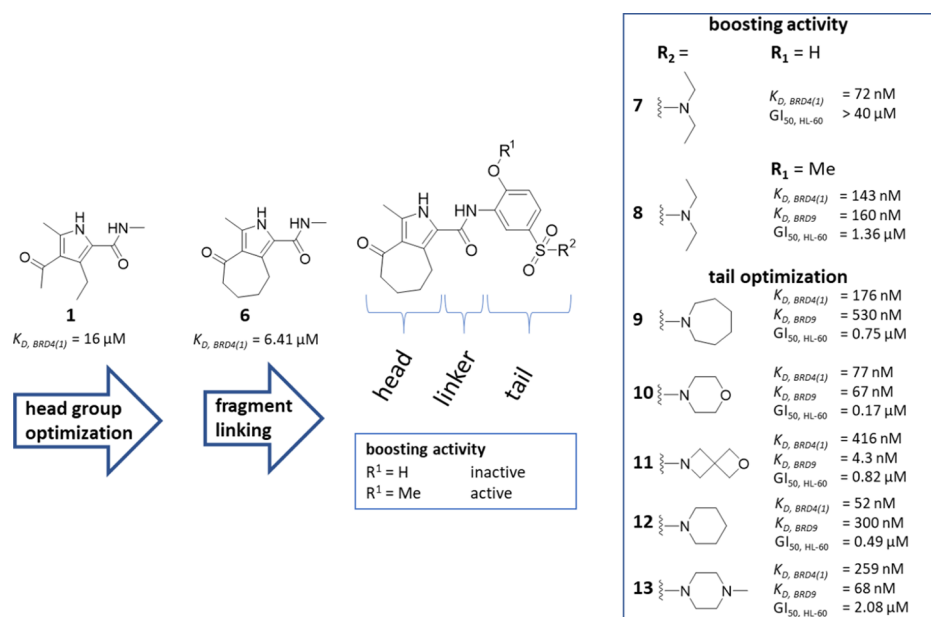


Figure 1. Evolutionary history of the ligands 6–13. Fragment 1 was optimized to 6 in a first step. The subsequent fragment linking with the tail of 2 (Table 1) resulted in inhibitor 7. In the case of 8, the change of R₁ from H (7) to Me resulted in a significant increase in activity. The final modifications performed on R₂ resulted in the inhibitors 9–13. They all show nanomolar affinities to BRD4(1) and BRD9. Furthermore, inhibitors 9–12 show GI_{50,HL-60} values in the nanomolar range.

compared to its progenitors 2 and 6. In a next step, the selectivity of 7 was analyzed in a selectivity screen against a selection of the known human BDs (bromoMAX, DiscoverX; Supporting Table S6). The screening discloses a clear preference for the BET family with BRD7, BRD9, BRPF1B, and CBP as additional targets (ratio of the average percent control of the BET-BDs excluding BRDT to tested BDs <10). The resulting profile is highly comparable to the previously shown profile of 2¹³ although the activities for 7 are much higher (Supporting Table S5). However, the GI values of 7 do not fully reflect the low K_D, BRD4(1). Previously, a similar behavior was observed for 2.¹³

2.3. Boosting Activity. A possible reason for the relatively low activity of 2 and 7 was assumed to be poor membrane permeability as well as a possibly rapid modification and subsequent excretion due to the phenolic hydroxyl group²⁷ (Figure 1). To validate this hypothesis, the methoxy analogue of 7 was synthesized (8). The structure of 8 in complex with BRD4(1) (Figure 2C) shows only minor deviations as compared to 7 (Figure 4A). ITC revealed an affinity that was about two times lower as for the predecessor 7 (Tables 2 and 3). However, a comparison of the NCI60 profiles and GI₅₀ values shows a significantly increased activity of 8 over 7 (Table 2 and Supporting Table S5). This is also reflected by the low GI₅₀ values for several cancer cell lines (Table 2 and Supporting Table S5).

2.4. Tail Optimization: Closing the Second Ring. Following the success of the ring closure on the pyrrole part, we applied this optimization strategy also to the tail (Figure 1). For this purpose, we applied moieties that have been discovered in a previous study.¹⁴ The combination of the sulfonamide parts of 4 and 5, respectively, with 8 yielded the ligands 9 and 10 (Figure 2D,E). Crystal structures with BRD4(1) show that, compared to 8, the sulfonamide is rotated by 180°, and the aromatic plane is rotated along the N-aryl bond. This allows for additional hydrophobic interactions of the ligand-tails with the ZA-loop. The lower space requirement of the morpholine tail of

10 results in a reduced rotation of the aromatic plane of about 30° as compared to the azepane tail of 9 (about 37°). The seven-membered ring of the head group of 9 is slightly different from those of 8 and 10.

In fact, the positioning of 9 resembles the binding behavior of 4 (Figure 4B). In contrast, 10 does not reproduce the binding mode of 5. This can be explained by the substantially differing electron density distribution in the aryl and its influence on the binding mode within the WL-trap¹⁴ (Figure 4C). ITC showed for 9 a decrease in affinity to BRD4(1) compared to 8, whereas 10 showed a clear improvement (Tables 2 and 3). The next generation, 11 (Figure 2F) and 12 (Figure 2G), represents combinations of the tails of 9 and 10, where 11 combines the properties of the morpholine residue of 10 with the slightly higher space requirement of 9 while retaining the ether function. In addition, the spiro moiety replacing the morpholine should contribute to stability with otherwise comparable properties.^{28–30} 11 shows a very similar binding behavior compared to 9 (Figure 4D). Both the head group and the aryl part are placed almost identically in the binding pocket. Compared to 9, mainly the tail differs, which in the case of 11 with its oxetane comes closer to Asp88 at the ZA loop, thus establishing hydrogen bonds to surface waters (Figure 2F). Overall, the affinity to BRD4(1) decreases noticeably due to the modification, while the affinity to BRD7/9 reaches its maximum among the inhibitors presented here (Tables 2 and 3, and Supporting Table S8). With 12, the hydrophobic character of the azepane tail (9) was combined with the smaller space requirement of the morpholine tail (10). The resulting binding mode of the piperidine tail of 12 (Figure 2G) is almost identical to that of 10 (Figure 4E). For 12, ITC showed the highest affinity to BRD4(1) of all inhibitors presented in this study (Tables 2 and 3).

2.5. Targeting Trp81. With 13, a ligand was designed which should not bind to the hydrophobic region of the ZA loop addressed by 9 and 10 but should rather establish a cation–π

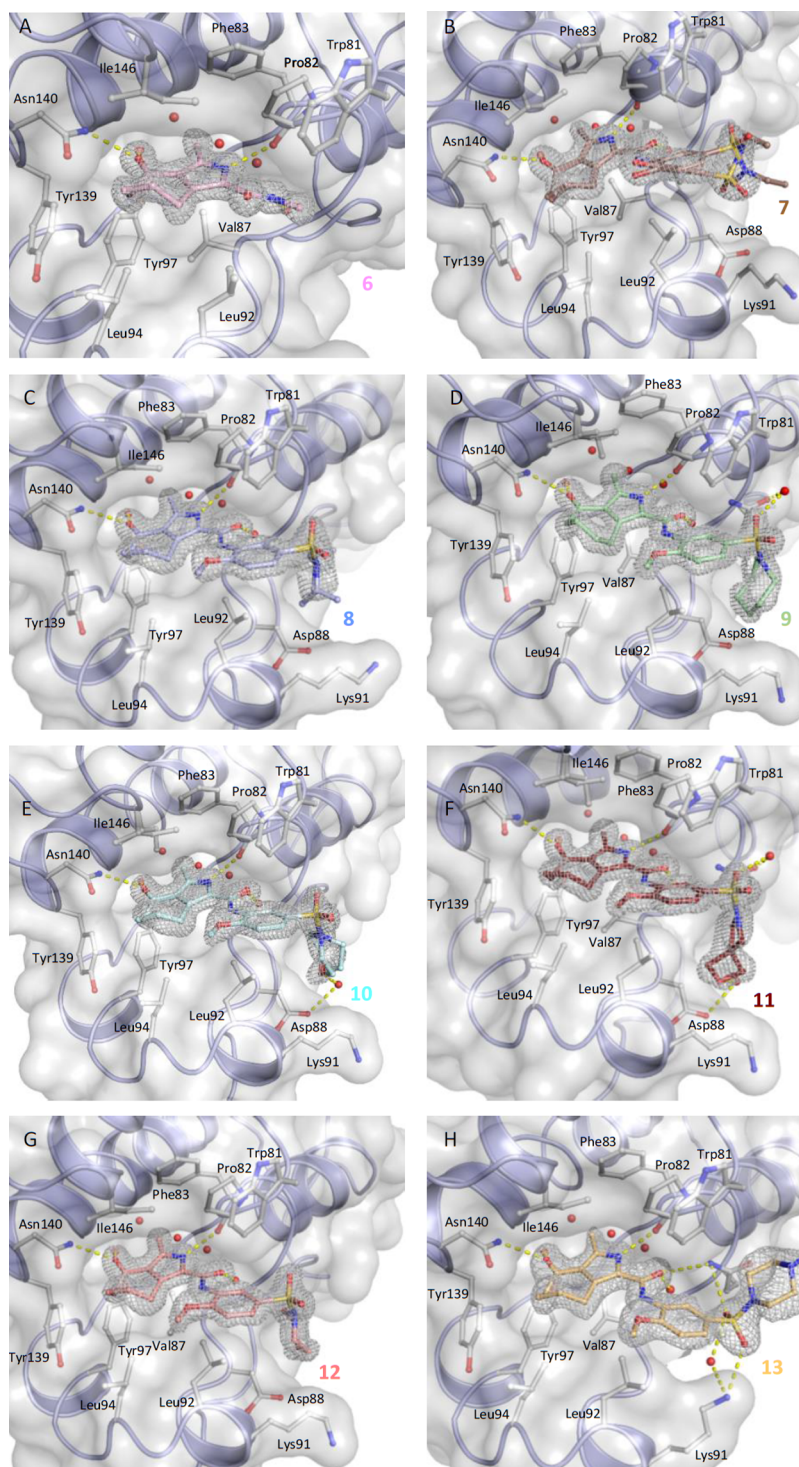


Figure 2. Crystal structures of **6–13** (PDB IDs 6RWJ, 6SB8, 6S4B, 6S6K, 6SA2, 6SAH, 6SAJ, and 6SA3; A–H) in complex with BRD4(1). The protein is shown as a cartoon with a solvent accessible surface. Conserved waters and ligand–protein bridging waters are shown as red spheres. Side chains of interest as well as the ligands are shown as ball-and-stick. Hydrogen bonds are indicated by dashed yellow lines. The electron density map is shown as a 2Fo-Fc omit map contoured at 1.0 σ . All structures show a similar binding mode for the 4-acyl pyrrole, the amide linker, and the phenyl part. In all cases, hydrogen bonds are formed from the 4-acyl pyrrole to the side chain of Asn140, as well as to the carbonyl of the peptide backbone of Pro82. The following amide linker forms a hydrogen bond to the fifth conserved water within the binding pocket, and the phenyl part is always positioned in the WL-trap.¹³

interaction between Trp81 and its methylpiperazine moiety. The desired binding mode could be confirmed experimentally (Figure 2H). The head and the linker bind as already shown for the other representatives. The sulfonamide is oriented as in **7** and **8**. Compared to **8**, a rotation of the aromatic plane along the

N-aryl bond (approx. 25°) can be observed. This leads to an improved surface complementarity of the 1-methylpiperazine tail to Trp81 as well as a cation– π interaction (distance <6 Å). However, ITC with BRD4(1) revealed a significantly reduced affinity compared to the previous ligands (Tables 2 and 3).

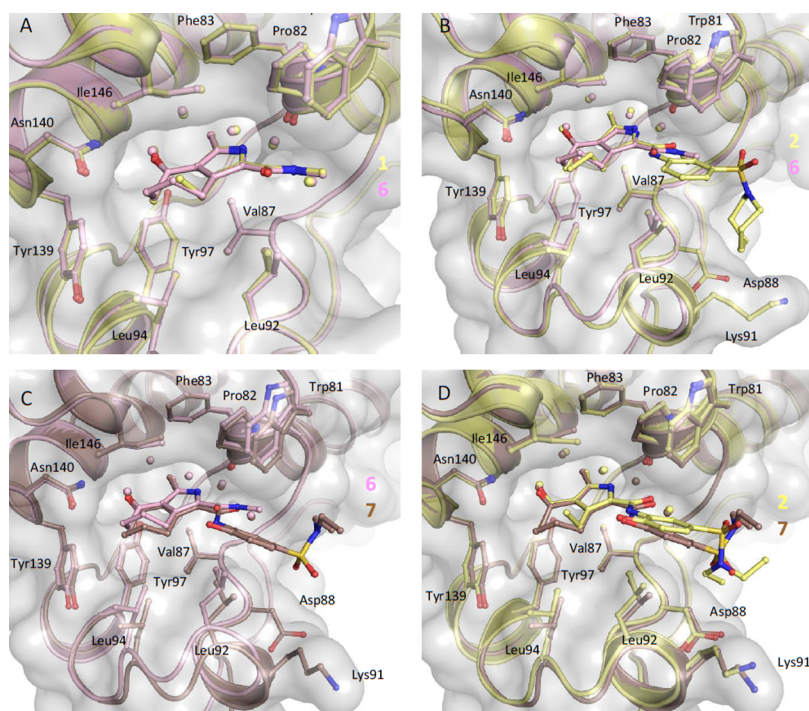
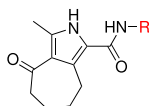


Figure 3. Superposition of ligands and their progenitors bound to BRD4(1). The protein is shown as a cartoon with a solvent accessible surface. Conserved waters are shown as spheres in the color of the corresponding protein and ligand. Side chains of interest as well as the ligands are shown as ball-and-stick. (A) Superposition of the 4-acyl pyrrole-based fragments **1** and **6** reveals a highly similar binding mode (PDB IDs 4LZS and 6RWJ). (B) The superposition of **4** (PDB ID 5D3R) and **6** shows a slightly differing binding mode of the 3-alkyl moiety, due to the ring closure in **6**. (C) The headgroup of **7** (PDB ID 6SB8) shows a highly similar binding mode as compared to the fragment **6**. (D) **2** (PDB ID 4LYW) and **7** bind highly similar with only minor deviations.

Table 2. Affinities to BRD4(1) and BRD9 and GI₅₀ for Successors of **2** (**6**–**13**).^a



#	R	K _D [nM]		GI ₅₀ [μM]		
		BRD4(1)	BRD9	HL-60	MCF-7	SK-MEL-5
6	Me	*6,410	n.d.	n.d.	n.d.	n.d.
7		*72	n.d.	> 40	> 40	> 80
8		85	160	1.36 ± 0.20	6.84 ± 0.52	16.3 ± 3.9
9		170	530	0.565 ± 0.077	3.00 ± 0.43	6.85 ± 0.79
10		60	67	0.170 ± 0.043	7.67 ± 1.36	6.80 ± 1.21
11		150	4.3	0.821 ± 0.212	5.76 ± 0.30	20.8 ± 6.9
12		82	300	0.491 ± 0.065	4.06 ± 1.06	6.79 ± 2.93
13		300	68	2.08 ± 0.16	> 25	> 20

^aAffinities were determined via bromoKdELECT (DiscoverX), except for those * marked, which were determined using ITC. For GI₅₀ values determined by us, the standard deviations are given.

Table 3. Binding Parameters of BRD4(1) with Ligands Determined by ITC^a

#	K_D [μ M]	ΔG [kcal/mol]	ΔH [kcal/mol]	ΔS [cal/mol·K]	$P99\%_{k_D}$ [μ M]	$P99\%_{\Delta H}$ [kcal/mol]
6	6.41	−7.09	−9.58	−8.37	4.62–7.94	−10.2 to −8.48
7 _{15°C}	<0.01	−11.0	−12.1	−3.83	<<0.01–0.04	−14.0 to −10.4
7 _{25°C}	0.07	−9.74	−16.4	−22.4	0.06–0.08	−16.6 to −16.2
7 _{37°C}	0.17	−9.59	−21.9	−39.5	0.13–0.23	−23.1 to −20.7
8	0.14	−9.33	−12.4	−10.4	0.10–0.20	−13.0 to −11.9
9	0.18	−9.21	−11.2	−6.51	0.12–0.25	−11.7 to −10.6
10	0.08	−9.70	−13.2	−11.8	<0.01–0.12	−14.2 to −12.4
11	0.26	−8.99	−9.84	−2.87	0.21–0.32	−10.2 to −9.49
12	0.05	−9.93	−14.3	−14.8	0.04–0.06	−14.4 to −13.6
13	0.42	−8.70	−11.7	−10.2	0.30–0.59	−12.7 to −10.9

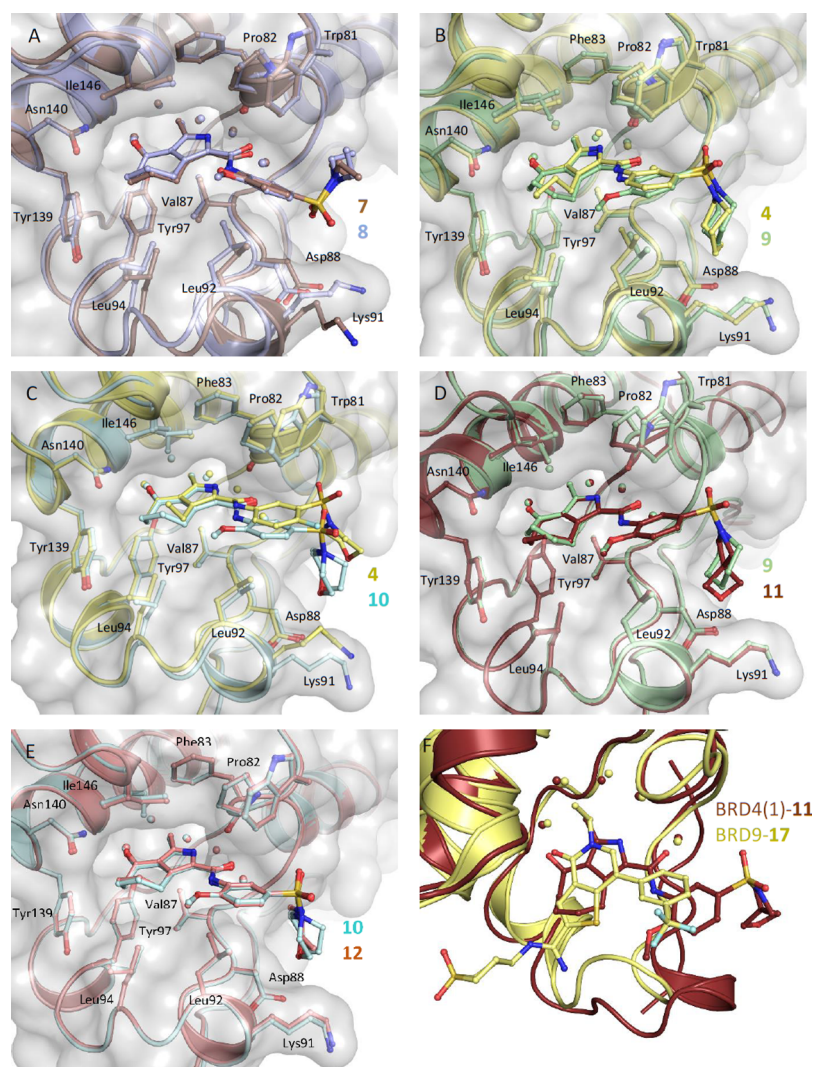
^aITC was carried out at 25 °C, if temperature is not specified.

Figure 4. Superposition of ligands and their progenitors bound to BRD4(1), as well as of 9, 10 and 12. The protein is shown as a cartoon with a solvent accessible surface. Conserved waters and ligand–protein bridging waters are shown as red spheres. Side chains of interest as well as the ligands are shown as ball-and-stick. (A) Methylation of the hydroxy group of 7, yielding 8, has very little influence on the binding mode (PDB IDs 6SB8 and 6S4B). (B) 9 mostly reproduces the binding mode of 4 in defiance of the missing methoxy group (PDB IDs 6S6K and 5D3R). (C) Binding mode, as well as the electron distribution in the aryl tail, of 10 (PDB ID 6SA2) and 4 differ clearly. (D) Superposition of 9 and 11 reveals a highly comparable binding mode, despite the slightly longer spiro tail of 10 (PDB ID 6SAH). (E) Replacing the morpholine tail of 10 by a piperidine, yielding 12 (PDB ID 6SAJ), has only little influence on the binding mode. (F) Superposition of 11 bound to BRD4(1) and 17 bound to BRD9 (PDB ID 4UIW) reveals the 5-alkyl pyrrole as a potential selectivity regulator.

2.6. Negative Control. With 14, the negative control of 12 was realized. For this purpose, the pyrrole nitrogen was

methylated to force 14 to clash with the backbone carbonyl oxygen of Pro82. Due to the modification, the activity and

Table 4. Affinities to BRD4(1) and BRD9 and GI₅₀ Values for Diverse Known BD Inhibitors and the Negative Control of 12, 14.^a

#	Structure	K_D [nM]		GI ₅₀ [μ M]		
		BRD4(1)	BRD9	HL-60	MCF-7	SK-MEL-5
2 (XD14)		160 ^[13]	n.d.	17 ^[13]	n.d.	n.d.
14		no binding	n.d.	>> 10	>> 10	>> 10
15 ((+) -JQ1)		13 ^[31]	weak / no binding ^[8]	0.021 ± 0.004	> 50	> 40
16 (TP 472)		> 990 ^[22]	*33 ^[22]	1.33 ± 0.15	4.49 ± 1.06	2.77 ± 0.15
17 (I-BRD9)		1400 ^[23]	1.9 ^[23]	+0.433 ^[25]	n.d.	n.d.
18 (LP99)		weak / no binding ^[32]	*99 ^[32]	+5.03 ^[25]	n.d.	n.d.
19 (GNE-375)		° > 20 ^[24]	5 ^[24]	n.d.	~1.34 ^[24]	n.d.
20 (I-CBP 112)		*5600 ^[33]	weak / no binding ^[33]	> 50 ^[33]	> 50 ^[33]	> 50
21 (XDM-CBP)		> 4000 ^[20]	2900 ^[20]	1.3 ^[20]	4.2 ^[20]	4.2 ^[20]

^aAffinities were determined via bromoKdELECT (DiscoverX), except for those * marked or °, which were determined via ITC or TR-FRET,²⁴ respectively. For GI₅₀ values determined by us, the standard deviations are given. + marked or ~ marked GI₅₀ values were determined after 7²⁵ or 8²⁴ days, respectively.

affinity to BRD4(1) as well as the solubility decreases; hence a maximum concentration of 10 μ M was used for the measurements. At this concentration, no binding to BRD4(1) could be detected by ITC, and the growth of HL-60, MCF-7, and SK-MEL-5 is little to not affected (Table 4, Supporting Figure S119). This suggests a robust selectivity of 12 toward BDs over non-BD off-targets in the tested cell lines.

2.7. Specificities and Off-Targets within the BD Family.

A BD inhibition profile including 32 human BDs (bromoMAX, DiscoverX) was obtained for compounds 1, 6, 7, and 10

(Supporting Table S8). Since all profiles were determined at different test concentrations, a direct comparison has been done via calculated Z-scores (deviation from mean value in standard deviations). All four activity profiles are very similar, although the fragments 1 and 6 exhibit lower specificity. Due to the very strong inhibition of the BET family, 10 yields full inhibition at the tested concentration (percent control = 0). BRPF1, a target outside the BET family, is strongly addressed by all tested compounds. In addition, 6, 7, and 10 clearly address BRD7 and BRD9. For further characterization, the K_D s for 10 were

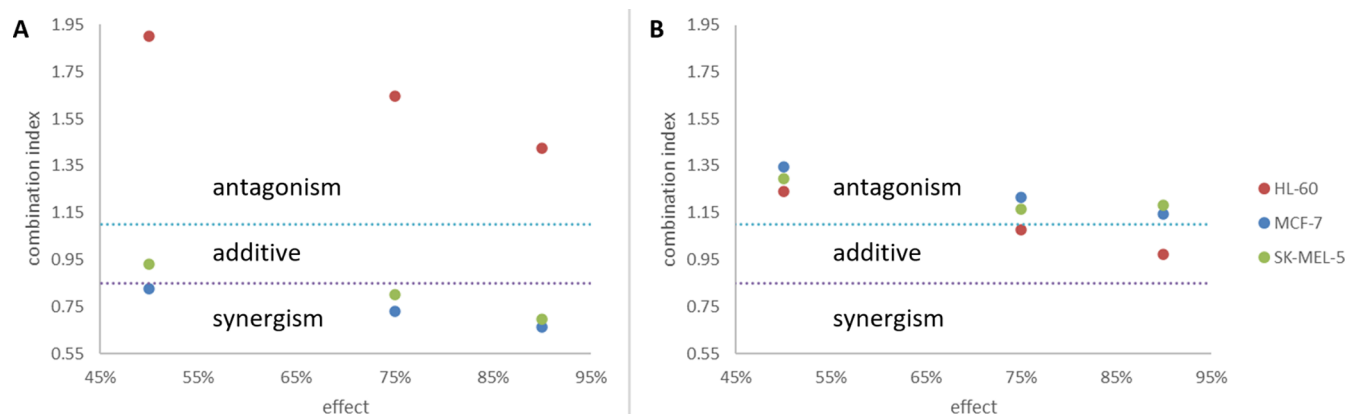


Figure 5. Combination index^{35,36} for HL-60, MCF-7, and SK-MEL-5 with **15** ((+)-JQ1) and **18** (LP99) at 50, 75, and 90 percent growth inhibition. The combination index indicates a synergistic effect for values smaller than 0.85, an antagonistic effect for values larger than 1.1 and a mostly additive effect in between.³⁶ Borders are indicated by dotted lines. Values for HL-60 are shown as red spheres, for MCF-7 as blue spheres, and for SK-MEL-5 as green spheres. (A) Concentration of **18** was kept constant at approximately 50% of its individual GI_{50} (5 μ M for HL-60, 18 μ M for MCF-7, and 10 μ M for SK-MEL-5). (B) Concentration of **15** was kept constant at approximately 10% of its individual GI_{50} (10 nM for HL-60, 30 nM for MCF-7 and 90 nM for SK-MEL-5).

determined for the BET family, BRD7, BRD9, and BRPF1 (Supporting Table S9) by means of the bromoKdELECT assay. The affinities match the bromoMAX profile very well and confirm BRD7 and BRD9 as additional strong targets (K_D ratio of BRD7 and BRD9 to BRD4(1) = 1.4 and 1.1, respectively). Although the affinity is also in the nanomolar range, BRPF1 is substantially less inhibited (K_D ratio of BRPF1B to BRD4(1) = 8.7).

To further characterize the specificity of **8**, **10**, **11**, **12**, and **13**, we selected all BDs with percent control <2% from the previously obtained profile of **10** (Supporting Table S8) for K_D determination. Thus BRD4(1), as representative of the BET family, as well as BRD7, BRD9, BRPF1, CECR2, and EP300, were selected for a bromoKdELECT assay (DiscoverX) (Supporting Table S9). The results mostly confirm the affinities to BRD4(1) previously determined experimentally by ITC (Table 3). Furthermore, all inhibitors tested show K_D s in the nanomolar range for BRD7 and BRD9, with **12** having the lowest and **11** the highest affinity. In comparison with the affinities to BRD4(1), only little selectivity is observed. In the case of **11** and **13**, BRD7 and BRD9 are even better addressed than BRD4(1), with **10** even showing moderate selectivity for BRD7 and BRD9 over BRD4(1) (K_D ratio (bromoKdELECT) BRD4(1) to BRD9 = 34.9). p300 is bound in the low micromolar to high nanomolar range (not tested for **10**). With the high affinity to BRD4(1), however, the tested inhibitors, except for **11** and **13**, show at least 24-fold selectivity for BRD4(1) over p300. For BRPF1 and CECR2, the picture is more heterogeneous. While **9**, **11**, and **12** exhibit moderate to good selectivity for BRD4(1) for both BDs (BRPF1 is bound in the micromolar range, CECR2 in the high nanomolar range with **9** being the most selective), **13** fails to establish a good selectivity. Quite surprisingly, although being unable to discriminate BRD4(1) against BRPF1, **8** shows pronounced selectivity for BRD4(1) over CECR2, only outrun by **9**.

2.8. Activities on a Broader Panel of Cancer Cell Lines.

8, **10**, **11**, **12**, and **13** were tested by National Cancer Institute (NCI, NIH, Rockville, MD, US) on a defined broad panel of cancer cell lines (NCI60 panel,³⁴ Supporting Table S5). In terms of addressed cell lines, all inhibitors showed similar profiles with minor deviations. However, with respect to cellular efficacy,

there are more substantial differences: **7**, **13**, and partly **11** are the least active inhibitors, while **8**, **9**, and **12** are notably more active. Based on the average Z score (Supporting Table S6) of the GI values (growth inhibition at 10 μ M for 72 h, GI > 100% indicate lethality), the cancer cell lines SK-MEL-5 (melanoma), HL-60 (leukemia), LOX IMVI (melanoma), SNB-75 (CNS cancer), and MDA-MB-468 (breast cancer) are addressed most strongly (Supporting Table S5). Remarkably, although harboring a generally weak antiproliferative effect just like **7**, **11** peaks for HL-60 on a level that is comparable to the much more potent ligand **12** ($GI_{11,HL-60}$ = 111% with a Z score of 3.13 and $GI_{12,HL-60}$ = 111% with a Z score of 1.68, Supporting Table S6). The latter proved to be the most active compound, and hence it was selected by the NCI for a refined five dose testing. GI_{50} , TGI, and LC_{50} were determined for the entire NCI60 panel (Supporting Tables S5 and S6). A GI_{50} value in the nanomolar range was found for 17 cancer cell lines, including CNS cancer, melanoma, renal cancer, or breast cancer. The most sensitive cell lines are SNB-75 (141 nM), UACC-62 (355 nM), and NCI-H522 (372 nM). The LC_{50} s for most cancer cell lines were above the measured maximum concentration of 100 μ M, but some were in the low micromolar range, for example, LOX IMVI (8.17 μ M), SK-MEL-5 (12.2 μ M), and A498 (19.7 μ M).

Finally, GI_{50} values were determined for the cancer cell lines HL-60, MCF-7, and SK-MEL-5 with **8**–**13** (Table 2). HL-60 was chosen because of its high sensitivity to BET inhibition and the inhibitors presented here. MCF-7 and SK-MEL-5 were chosen because of their insensitivity to BET inhibition and their sensitivity to the above described inhibitors.³¹ In order to differentiate between the effects of BRD7/BRD9 inhibition and those of BET-BD inhibition, GI_{50} values were additionally determined for **15** ((+)-JQ1⁸) as a pan-selective BET-BD inhibitor, **18** (LP99³²) as a selective BRD7/BRD9 inhibitor, and **16** (TP 472²²) as a moderately selective BRD7/BRD9 inhibitor. For a comparison of the effects of different BD inhibitors, the ligands **20** (I-CBP112),³³ a selective CBP/p300 BD inhibitor, and **21** (XDM-CBP), a less selective CBP/p300 BD inhibitor, were tested on SK-MEL-5. The results (Table 2) on HL-60 for **9**, **10**, **11**, and **12**, as well as for **15** showed GI_{50} values in the nanomolar range and for **8** and **13**, as well as for **16** in the low single digit micromolar range. All ligands were able to reduce

viability below 20% (Supporting Figures S92–S99). The picture is different for MCF-7 and SK-MEL-5. While the viability was reduced below 40% with **11** (Supporting Figure S103) and **16** (Supporting Figure S107), the others reduced viability even below 20% (Supporting Figures S100–S104). **15** was not able to reduce viability below 60% (maximum concentration tested = 50 μ M, Supporting Figure S106). On SK-MEL-5, the ligands **8**–**12** showed GI_{50} values in the low micromolar range with viability reduced below 20% (Supporting Figures S108–S112). **13** shows for MCF-7 and SK-MEL-5 only limited activity, but its poor solubility prevented a reliable determination of GI_{50} values (Supporting Figures S105 and S113). **15** leads to a reduction of viability even at low concentrations. However, this stagnates at approx. 70% up to a concentration of 25 μ M. At 50 μ M and above, a very rapid decrease in viability is observed (Supporting Figure S114). **16**, on the other hand, shows the best $GI_{50,SK-MEL-5}$ (2.77 μ M) of the compounds tested in this study. However, **16** does not succeed in lowering the viability below 26%, and for concentrations above 30 μ M, even a slow and steady increase in viability was observed (Supporting Figure S115).

2.9. Synergy of BET and BRD7/9 Inhibition. To validate a synergistic effect of BET and BRD7/9 inhibition, the combination index (CI)^{35,36} for the BET inhibitor **15** ((+)-JQ1) and the BRD7/9 inhibitor **18** (LP99) on HL-60, MCF-7, and SK-MEL-5 was determined (Figure 5 and Supporting Information Table S10). For this purpose, the CI was determined at 50, 75, and 90% effect, and the average was taken (Supporting Table S10).³⁶ While the combinations of **15** with constant concentration of **18** (approximately 50% GI_{20} , 5 μ M for HL-60, 18 μ M for MCF-7 and 10 μ M for SK-MEL-5; Figure 5A) show a synergistic effect on MCF-7 (average CI = 0.74) and SK-MEL-5 (average CI = 0.81), only antagonistic effects were found for HL-60 (average CI = 1.66). At a constant concentration of **15** (approximately 10% GI_{50} , 10 nM for HL-60, 30 nM for MCF-7, and 90 nM for SK-MEL-5) in combination with **18** (Figure 5B), only antagonistic effects were found (average CI_{HL-60} = 1.10, average CI_{MCF-7} = 1.24, and average $CI_{SK-MEL-5}$ = 1.21).

3. DISCUSSION

Our efforts to design BD inhibitors with enhanced activity yielded a number of novel inhibitors with remarkable properties. The ring closure in **1** yielding **6** successfully increased the affinity to many BDs, as can be seen from the respective single dose measurements (Supporting Table S8). Based on the ITC results for BRD4(1) (Table 3), this gain can be attributed to the significant improvement of ΔS from **6** to **1** (ΔS_6 = -8.37 cal $^{-1}$ K $^{-1}$, ΔS_2 = 26.5 cal mol $^{-1}$ K $^{-1}$), which is based on the reduction of degrees of freedom. As we already showed for **1**,^{13,20} a non-selective fragment can be used to generate much more specific inhibitors with a reasonable effort. This predestines **6** as a new, high-affinity fragment for the development of new BD inhibitors.

Ligand **7**, which was created by linking **6** to the tail of **2**, could increase affinity. Yet it still shows, just like **2**, a large gap between K_D and GI_{50} , which indicates a general problem with membrane permeability and/or stability. The free phenolic hydroxyl group was hypothesized to be the main problem in this context. The comparison of the cellular activity of **8**, the methoxy derivative of **7**, compared to **2** and **7** (Tables 2 and 4), largely confirms this. Other substitutions aside from methoxy have not been explored here but might be good starting points for further optimization steps, such as with the hydroxyl group pointing to the direction of solvents, it might be possible to create a prodrug, a bivalent

inhibitor,³⁷ a PROTAC,^{38,39} or a dual inhibitor^{40–42} in addition to classical ligand improvements.

Concerning the ring closure at the sulfonamide, the affinities to BRD4(1) of those ligands for which complex structures are shown here, suggest that six-membered rings are presumably favored over seven-membered rings or spiro compounds, as they may allow for a better interaction of the tails with the hydrophobic region in the ZA-loop. Furthermore, the increased space requirement of bulkier substituents might lead to a deviation of the ideal position of the aryl in the WL-trap, which in turn would lead to a reduction in ΔH and, more importantly, in ΔG . Ligand **13** forms an exception since its binding mode is significantly different compared to other ligands of the series.

It does not seem to matter for BRD4(1) whether hydrogen bonds at the tail are possible (**10**, **11**, and **13**) or not (**8**, **9**, and **12**), which is completely different for BRD9. Here, it seems to be the key to high affinities, while with increasing size and hydrophobicity of the tails, a significant reduction of affinity is found. In comparison to **8**, it becomes apparent that, in terms of affinity to BRD7/9, ring closures on the sulfonamide are only favorable if the resulting ring can form hydrogen bonds. A reasonable explanation for this can be given by the model structure of **11** with BRD9 (Figure 6). The model suggests a

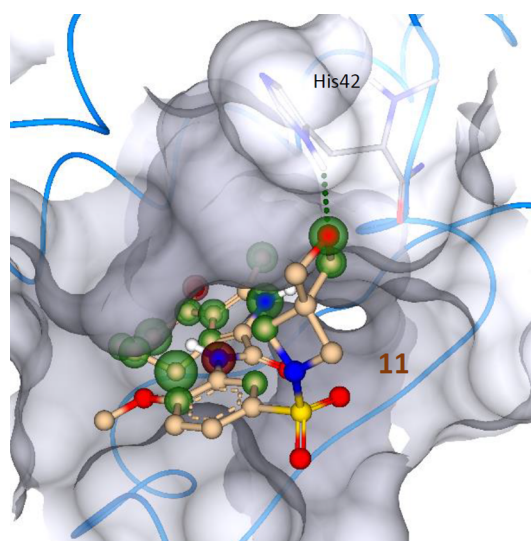


Figure 6. Modeled complex of BRD9 (PDB ID 4UIW) with **11**. The terminal oxygen shows a positive influence on affinity and forms a hydrogen bond to His42. Green spheres indicate positive and red spheres, a negative influence on affinity. Green dotted lines represent strong hydrogen bonds.

hydrogen bond to His42, and in combination with the affinities for BRD9, it can be assumed that the increased length of the tail of **11**, compared to **10** and **13**, has a positive effect on the affinity.

The BD inhibition profiles of **8**–**13** (Table 2) suggest that further modifications to the sulfonamide tail can further optimize affinity for individual BDs. For instance, in the ZA-loop of BRD4(1), Lys91, which is missing in BRD7/9, could form a cation– π interaction with an aromatic tail attached to the sulfonamide. Furthermore, the work of Crawford et al.²⁴ or the comparison with **17**²³ (Figure 4) suggests that modifications in the 5-pyrrole position should significantly increase specificity. However, many other optimization steps can be imagined, and a higher specificity does not necessarily have to be accompanied by a better activity.

The comparison of the given activities with the associated affinities confirms that within the BDs, the BET family has the biggest, yet not exclusive, impact on the cell growth of various tested cancer cell lines. However, in the case of very selective BRD9 inhibitors, this is only apparent after a longer incubation period (>3 days).^{24,26} Noteworthy, especially the very specific binders show a more limited activity profile. Thus, the pan-selective BET-BD inhibitor **15** ((+)-JQ1) shows only a very weak effect on MCF-7 and SK-MEL-5, and the highly specific BRD7/9 inhibitors **17–19** (I-BRD9, LP99 and GNE-375) show nearly no growth inhibition after three days incubation; and the highly specific CBP/p300 inhibitor **20** (i-CBP 112) also shows no effect on HL-60, MCF-7, or SK-MEL-5. However, the much less selective binders **16**, **21**, and **8–12** all show a stronger effect on these three cell lines after three days. Furthermore, only the novel dual inhibitors presented here show a reduction in viability of more than 80% on MCF-7 and SK-MEL-5. These findings are in perfect agreement with the work of Crawford et al.,²⁴ who identified the need for longer incubation times for selective BRD7/9 inhibitors, as well as with the work of Bevill et al.²⁶ who showed recently a synergistic effect for the inhibition of BDs of BET, BRD7/9, and CBP/p300 on various breast cancer cell lines. Remarkably, the K_D ratio of BET to BRD9 already allows an estimation of potency on MCF-7 and SK-MEL-5. Very specific BRD7/9 or BET inhibitors (K_D ratio >100) show little or no effect, while dual inhibitors (K_D ratio close to 1) show the most pronounced effect. Noteworthy, a strong decrease in viability below 20% could only be observed for the dual BET-BRD7/9 inhibitors but not for the combination of the BET inhibitor **15** and BRD7/9 inhibitor **18** (Supporting Table S10). The combination experiments for **15** with a fixed concentration of **18** suggest that the observed effects of **8–12** on MCF-7 and SK-MEL-5 is due to synergism of BET-BRD7/9 dual inhibition. Since the inhibitors presented here (**8–12**) also address other BDs (e.g. BRPF1B, CBP/p300), further synergistic effects cannot be completely excluded or in the case of CBP/p300 can even be expected.²⁶ This is in well agreement with a comparison of highly BD selective (**15**, **17–20**) as well as less selective BD inhibitors (**8–12**, **16** and **21**), as only the less specific inhibitors show a fast and strong effect on MCF-7 and SK-MEL-5 (Tables 3 and 4). The fact that only antagonistic effects were found for the combination of **18** with fixed concentrations of **15** is probably due to the fact that BRD7/9 inhibitors alone hardly show any effect. The activities found in the high double-digit micromolar range are probably due to off-target effects, as BRD7/9 should have been completely blocked much earlier. This identifies BRD7/9 inhibitors as potential enhancers of BET inhibitors on BET inhibition insensitive cancer cell lines, which is also in good agreement with the finding that the unselective or dual inhibitors have a very strong effect on MCF-7 and SK-MEL-5. Off-targets besides the BDs cannot be completely ruled out but appear unlikely due to the similar effects on cell viability with substantially different scaffolds structures (e.g. **16** vs **8–12**). This is further supported by the negative control of **12** (**14**) since this very similar compound does not show affinity for BRD4(1) but also no activity against any assayed cancer cell lines.

In conclusion, this study not only presents a set of potent and highly cell active BET-BRD7/9 BD inhibitors but it also sheds light on the importance of BD inhibition profiles as crucial key players in addressing various cancer types, which are not addressable with highly selective BD inhibitors alone. This is clearly demonstrated by the strong effect of dual BET-BRD7/9

BD inhibitors as well as the combination of selective BRD7/9 and BET inhibitors compared to the negligible effect of the single selective BD inhibitors on various cancer cell lines, such as SK-MEL-5 (melanoma) and MCF-7 (breast cancer).

4. EXPERIMENTAL SECTION

4.1. Ligand Design. The ligands were optimized on the basis of rational considerations and experience from former optimization campaigns on BRD4(1)^{13,14}.

4.2. Synthesis and Characterization. Reagents and solvents were obtained from commercial sources and used without any further purification.

Column chromatography was carried out using MACHEREY-NAGEL silica gel 60 (0.04–0.063 mm).

Thin layer chromatography (TLC) was performed on aluminum plates pre-coated with silica gel (MERCK, 60 F₂₅₄). TLC-monitored reactions were visualized by UV fluorescence ($\lambda = 254$ nm) and/or by staining with ninhydrine in EtOH or KMnO₄ in 0.5 M K₂CO₃.

NMR spectra were acquired on a BRUKER AVANCE 300 spectrometer (300 MHz), on a BRUKER AVANCE 400 spectrometer (400 MHz and 100.6 MHz for ¹H and ¹³C respectively), or on a Bruker 500 DRX NMR spectrometer with a TBI probe head (499.6 MHz and 125.6 MHz for ¹H and ¹³C respectively) at a temperature of 303 K unless specified. Chemical shifts are reported in parts per million (ppm) relative to the residual solvent. Data for ¹H NMR are described as follows: chemical shift (δ in ppm), multiplicity (s, singlet; d, doublet; t, triplet; q, quartet; m, multiplet; and br, broad signal), coupling constant (Hz), and integration. Data for ¹³C NMR are described in terms of chemical shift (δ in ppm).

Purity of the final compounds was determined to be $\geq 95\%$ by ¹H NMR on the Bruker 500 DRX NMR spectrometer as prescribed by the general guidelines for quantitative 1D ¹H NMR.

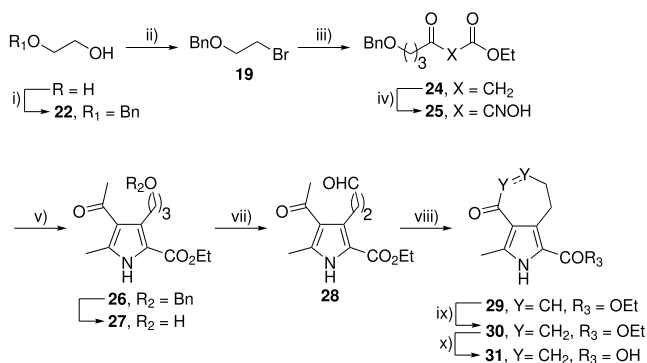
HRMS were obtained on a THERMO SCIENTIFIC Advantage and a THERMO SCIENTIFIC Exactive instrument (APCI/MeOH: spray voltage 4–5 kV, ion transfer tube: 250–300 °C, vaporizer: 300–400 °C).

Compound **6** was prepared starting from ethane-1,2-diol, protected by benzyl bromide (**22**), and then transformed to alkyl bromide (**23**) using *N*-bromosuccinimide and PPh₃. Treatment of ethyl acetoacetate in the presence of sodium hydride and *n*-BuLi to deprotonate the molecule twice, and then adding alkyl bromide **23**, led to alkylation at the more reactive site. Then, compound **24** was transformed to the corresponding oxime **25** by sodium nitrite in a mixture of acetic acid and water. Condensation of **25** with pentane-2,4-dione using zinc in acidic media afforded the pyrrole **26**, which was deprotected by hydrogenation using palladium on charcoal (**27**). Then, the aldehyde **28** was obtained using Swern reaction. Formation of the bicyclic pyrrole **29** was tried using various acids or bases, and PTSA monohydrate was found to be the most effective, providing the desired compound in moderate yield. Reduction of alkene **29** followed by ester hydrolysis of **30** in THF/H₂O enabled access to the corresponding acid **31** (Scheme 1).

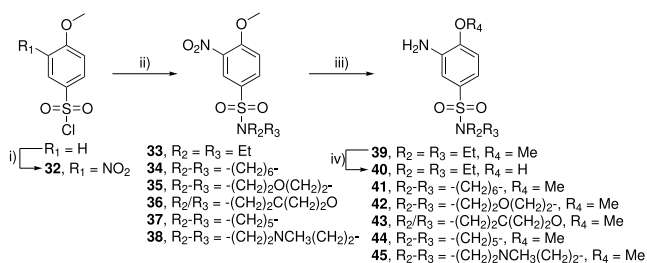
Synthesis of compounds **39–45** was done in three steps starting from nitration of 4-methoxybenzenesulfonyl chloride, followed by the formation of the sulfonamide (**33–38**) and reduction by hydrogenation using palladium on charcoal. Compound **39** was also demethylated by boron tribromide in dichloromethane to afford the sulfonamide **40**.

Methylamine and all previously synthesized anilines derivatives (**39–45**) were coupled to the pyrrole **31** using Ghosez's reagent (**6**, **11**, and **12**), CDI (**7**), or HCTU (**8–10** and **13**) (Scheme 2).

4.3. 2-(Benzyloxy)ethan-1-ol (22**).** The synthesis was done according to ACS Medicinal Chemistry Letters, **2016**, 7(2), 172–176 to give the desired product (14.4 g, 94.4 mmol, 81%) as a light yellow oil. ¹H NMR (400 MHz, CDCl₃): δ 7.39–7.27 (m, 5H), 4.56 (s, 2H), 3.79–3.69 (m, 2H), 3.61–3.54 (m, 2H), 2.61–2.50 (m, 1H); ¹³C NMR (101 MHz, CDCl₃): δ 138.0, 128.4, 127.8, 127.7, 73.2, 71.5, 61.8; R_f: 0.39 (40% AcOEt in PE).

Scheme 1. Synthesis of Pyrrole 31^a

^aReagents and conditions: (i) BnBr, NaH, THF, rt, 81%; (ii) NBS, PPh₃, CH₂Cl₂, -78 °C to rt, 89%; (iii) Ethyl acetoacetate, NaH, then *n*-BuLi, -20 °C to rt, 76%; (iv) NaNO₂, AcOH/H₂O, 0 °C to rt, 96%; (v) Pentane-2,4-dione, Zn, AcOH, AcONa, 90 °C, 63%; (vi) H₂, Pd/C, EtOAc/MeOH, rt, 67%; (vii) (COCl)₂, DMSO, NEt₃, CH₂Cl₂, -78 °C to rt, 88%; (viii) PTSA monohydrate, PhMe, 110 °C, 56%; (ix) H₂, Pd/C, EtOAc/MeOH, rt, 98%; (x) NaOH, EtOH/H₂O, reflux, then HCl, 0 °C, 71%.

Scheme 2. Synthesis of Aniline Derivatives 39–45^a

4.4. ((2-Bromoethoxy)methyl)benzene (23). To a solution of NBS (17.7 g, 99.3 mol, 1.0 equiv) in CH₂Cl₂ (200 mL) was added dropwise a solution of PPh₃ (26.1 g, 99.3 mol, 1.0 equiv) in CH₂Cl₂ (140 mL) at -78 °C. The solution was stirred for 1 h, and then a solution of 2-(benzyloxy)ethanol (14.4 g, 94.6 mmol, 1.0 equiv, 22) in CH₂Cl₂ (100 mL) was added dropwise. The solution was allowed to return to rt and after 1 h, and the reaction was quenched using MeOH (10 mL) and PhMe (150 mL). The solution was evaporated, water was added, and the aqueous phase was extracted three times with EtOAc. The combined organic layers were washed with brine, dried over Na₂SO₄, and evaporated. The residue was purified on silica gel column eluting with 10% EtOAc in CyH to afford the desired product (18.1 g, 84.1 mol, 8 9%) as a light yellow oil. ¹H NMR (400 MHz, CDCl₃): δ 7.41–7.28 (m, 5H), 4.60 (s, 2H), 3.80 (t, *J* = 6.2 Hz, 2H), 3.50 (t, *J* = 6.2 Hz, 2H); ¹³C NMR (101 MHz, CDCl₃): δ 137.9, 128.6, 127.9, 127.8, 73.2, 70.1, 30.5; *R*_f: 0.85 (20% AcOEt in CyH).

4.5. Ethyl-6-(benzyloxy)-3-oxohexanoate (24). Ethyl acetoacetate (32.2 mL, 252 mmol, 1.0 equiv) was added dropwise to a suspension of NaH (5.55 g, 278 mmol, 1.1 equiv, 60% w/w) in dry THF (500 mL) at -20 °C. The reaction mixture was stirred for 1 h, and then *n*-BuLi (2.5 M, 112 mL, 278 mmol, 1.1 equiv) was added dropwise. After 1 h, ((2-bromoethoxy)methyl)benzene (65.1 g, 302 mmol, 1.0 equiv, 23) was added, and the reaction mixture was allowed to return to rt and stirred overnight. A saturated NH₄Cl solution was added, and the organic phase was evaporated. The aqueous phase was extracted three times with EtOAc. The combined organic layers were

washed with brine, dried over Na₂SO₄, and evaporated. The residue was purified on silica gel column eluting with 10–100% EtOAc in PE to obtain the desired compound as an orange liquid (50.5 g, 191 mmol, 76%). ¹H NMR (300 MHz, CDCl₃): δ 7.38–7.26 (m, 5H), 4.47 (s, 2H), 4.18 (q, *J* = 7.1 Hz, 2H), 3.48 (t, *J* = 6.1 Hz, 2H), 3.43 (s, 2H), 2.66 (t, *J* = 7.1 Hz, 2H), 1.97–1.87 (m, 2H), 1.26 (t, *J* = 7.1 Hz, 3H); ¹³C NMR (101 MHz, CDCl₃): δ 202.6, 167.3, 138.5, 130.2, 128.5, 127.8, 127.8, 73.1, 69.2, 61.5, 49.5, 39.9, 23.9, 14.3; HRMS (pos. ESI): calcd for C₁₅H₂₀O₄Na M + Na⁺, 287.1254; found, 287.1254; *R*_f: 0.30 (20% AcOEt in CyH).

4.6. Ethyl 6-(benzyloxy)-2-(hydroxyimino)-3-oxohexanoate (25). To a solution of ethyl-6-(benzyloxy)-3-oxohexanoate (63.0 g, 238 mmol, 1.0 equiv, 24) in AcOH (240 mL) at 0 °C was added dropwise a solution of NaNO₂ (32.9 g, 477 mmol, 2.0 equiv) in H₂O (125 mL). The mixture was then allowed to return to rt and stirred overnight. Water was added, and the aqueous phase was extracted four times with EtOAc. The combined organic layers were washed three times with saturated Na₂CO₃ solution and brine and dried over Na₂SO₄ to afford the desired compound as a yellow oil (67.0 g, 229 mmol, 96%). ¹H NMR (400 MHz, CDCl₃): δ 10.51 (s, 1H), 7.42–7.26 (m, 5H), 4.53 (s, 2H), 4.35 (q, *J* = 7.1 Hz, 2H), 3.61–3.41 (m, 2H), 2.92 (t, *J* = 7.3 Hz, 2H), 2.09–1.78 (m, 2H), 1.33 (t, *J* = 7.2 Hz, 3H); ¹³C NMR (101 MHz, CDCl₃): δ 195.6, 161.9, 150.6, 137.5, 128.5, 127.9, 127.9, 73.0, 69.2, 62.2, 34.4, 23.6, 14.0; HRMS (pos. ESI): calcd for C₁₅H₁₉O₅NNa [M + Na]⁺, 316.1155; found, 316.1155; *R*_f: 0.63 (33% AcOEt in CyH).

4.7. Ethyl 4-Acetyl-3-(3-(benzyloxy)propyl)-5-methyl-1H-pyrrole-2-carboxylate (26). To a solution of ethyl 6-(benzyloxy)-2-(hydroxyimino)-3-oxohexanoate (28.1 g, 95.9 mmol, 0.8 equiv, 21) and pentane-2,4-dione (12.2 mL, 120 mmol, 1.0 equiv) in AcOH (275 mL) was added AcONa (39.3 g, 479 mmol, 4.0 equiv). The solution was heated to 90 °C, and Zn (19.6 g, 300 mmol, 2.5 equiv) was added portionwise. The reaction mixture was stirred for 1 h at 90 °C, filtered, and evaporated. Water was added to the residue, and the aqueous phase was extracted three times with EtOAc. The combined organic layers were washed with brine, dried over Na₂SO₄, and evaporated. The residue was dissolved in EtOAc and washed with aqueous citric acid solution (5%, w/v), saturated Na₂CO₃ (three times), and brine. The organic phase was dried over Na₂SO₄ and evaporated. The residue was quickly purified on a silica gel column eluting with 10–100% EtOAc in PE to afford the desired product as a yellow solid (20.9 g, 60.7 mmol, 63%). ¹H NMR (400 MHz, CDCl₃): δ 9.48 (br s, 1H), 7.40–7.27 (m, 5H), 4.51 (s, 2H), 4.31 (q, *J* = 7.2 Hz, 2H), 3.55 (t, *J* = 6.6 Hz, 2H), 3.21–3.07 (m, 2H), 2.52 (s, 3H), 2.46 (s, 3H), 1.93–1.78 (m, 2H), 1.33 (t, *J* = 7.1 Hz, 3H); ¹³C NMR (101 MHz, CDCl₃): δ 195.3, 161.7, 138.9, 138.0, 134.2, 128.3, 127.6, 127.4, 123.1, 118.0, 72.8, 70.5, 60.5, 31.4, 31.1, 22.7, 15.3, 14.4; HRMS (pos. ESI): calcd for C₂₀H₂₅O₄NNa [M + Na]⁺, 366.1676; found, 366.1676.

4.8. Ethyl 4-Acetyl-3-(3-hydroxypropyl)-5-methyl-1H-pyrrole-2-carboxylate (27). To a solution of ethyl 4-acetyl-3-(3-(benzyloxy)propyl)-5-methyl-1H-pyrrole-2-carboxylate (2.40 g, 6.99 mmol, 1.0 equiv, 26) in EtOAc and MeOH (28 mL, 1:1) under argon was added Pd/C (580 mg, 5% w/w). The solution was put under H₂ (1 atm) and stirred overnight at rt. The mixture was filtered over celite, evaporated, and purified on a silica gel column eluting with 50–100% EtOAc in CyH to afford the desired product (1.19 g, 4.70 mmol, 6 7%) as a light yellow solid. ¹H NMR (400 MHz, CDCl₃): δ 9.92 (br s, 1H), 4.31 (q, *J* = 7.2 Hz, 2H), 3.53 (dd, *J* = 6.1, 5.3 Hz, 2H), 3.36 (br s, 1H), 3.15 (t, *J* = 6.9 Hz, 2H), 2.54 (s, 3H), 2.44 (s, 3H), 1.89–1.72 (m, 2H), 1.34 (t, *J* = 7.1 Hz, 3H); ¹³C NMR (101 MHz, CDCl₃): δ 195.8, 161.6, 138.1, 134.5, 123.2, 118.4, 61.1, 60.6, 33.5, 31.1, 21.3, 15.5, 14.4; HRMS (pos. ESI): calcd for C₁₃H₁₉NO₄Na M + Na⁺, 276.1206; found, 276.1206; *R*_f: 0.42 (80% EtOAc in CyH).

4.9. Ethyl 4-Acetyl-5-methyl-3-(3-oxopropyl)-1H-pyrrole-2-carboxylate (28). To a solution of dry DMSO (3.93 mL, 55.3 mmol, 2.0 equiv) in dry CH₂Cl₂ (175 mL) was added dropwise oxalyl chloride (3.60 mL, 41.4 mmol, 1.5 equiv) at -78 °C. The reaction was stirred for 15 min. Afterward, a solution of ethyl 4-acetyl-5-methyl-3-(3-oxopropyl)-1H-pyrrole-2-carboxylate (7.00 g, 27.6 mmol, 1.0 equiv, 27) in dry CH₂Cl₂ (100 mL) was added dropwise and stirred for 30 min before NEt₃ (19.3 mL, 0.14 mol, 5.0 equiv) was added. The reaction

mixture was stirred for another 30 min at -78°C before it was allowed to return to rt. The solvent was evaporated, and H_2O was added. The aqueous phase was extracted three times with EtOAc, and the combined organic layers were dried over Na_2SO_4 , evaporated, and purified on a silica gel column eluting with 25–100% EtOAc in PE to afford the desired compound as a light brown solid (6.10 g, 24.3 mmol, 88%). $^1\text{H NMR}$ (400 MHz, CDCl_3): δ 9.81 (t, $J = 2.0$ Hz, 1H), 9.16 (br s, 1H), 4.33 (q, $J = 7.1$ Hz, 1H), 3.40 (dd, $J = 8.0, 7.1$ Hz, 2H), 2.69 (ddd, $J = 8.2, 7.1, 2.0$ Hz, 2H), 2.55 (s, 3H), 2.44 (s, 2H), 1.35 (t, $J = 7.1$ Hz, 2H); $^{13}\text{C NMR}$ (101 MHz, CDCl_3): δ 202.6, 194.7, 161.2, 137.3, 132.8, 123.1, 118.4, 60.8, 44.8, 31.2, 19.1, 15.7, 14.5; HRMS (neg. ESI): calcd for $\text{C}_{13}\text{H}_{16}\text{NO}_4 \text{M} - \text{H}^-$, 250.1085; found, 250.1085; R_f : 0.50 (50% AcOEt in CyH).

4.10. Ethyl 3-Methyl-4-oxo-2,4,7,8-tetrahydrocyclohepta[c]-pyrrole-1-carboxylate (29). To a solution of ethyl 4-acetyl-5-methyl-3-(3-oxopropyl)-1H-pyrrole-2-carboxylate (7.30 g, 29.1 mmol, 1.0 equiv, 28) in PhMe (291 mL) was added PTSA monohydrate (2.76 g, 14.5 mmol, 0.5 equiv). The mixture was heated to reflux for 3 h, cooled to rt, and evaporated. Concentrated NaHCO_3 solution was added, and the aqueous phase was extracted three times with EtOAc. The combined organic layers were washed with brine, dried over Na_2SO_4 , and evaporated. The residue was purified on a silica gel column eluting with 20–50% EtOAc in CyH to afford the desired product (3.79 g, 16.2 mmol, 56%) as a white solid. $^1\text{H NMR}$ (400 MHz, CDCl_3): δ 9.20 (br s, 1H), 6.63 (dt, $J = 12.3, 5.9$ Hz, 1H), 6.14 (dt, $J = 12.3, 1.5$ Hz, 1H), 4.33 (q, $J = 7.1$ Hz, 2H), 3.32–3.25 (m, 2H), 2.56 (d, $J = 0.6$ Hz, 3H), 2.53–2.45 (m, 2H), 1.37 (t, $J = 7.2$ Hz, 4H); $^{13}\text{C NMR}$ (101 MHz, CDCl_3): δ 188.8, 161.6, 143.9, 140.8, 134.4, 132.6, 123.6, 116.0, 60.6, 28.0, 24.5, 14.9, 14.6; HRMS (pos. ESI): calcd for $\text{C}_{13}\text{H}_{16}\text{NO}_3 \text{M} + \text{H}^+$, 234.1125; found, 234.1125.

4.11. Ethyl 3-Methyl-4-oxo-2,4,5,6,7,8-hexahydrocyclohepta[c]pyrrole-1-carboxylate (30). To a solution of ethyl 3-methyl-4-oxo-2,4,7,8-tetrahydrocyclohepta[c]pyrrole-1-carboxylate (3.50 g, 15.0 mmol, 1.0 equiv, 29) in EtOAc/MeOH (150 mL, 1:1) under argon was added Pd/C (700 mg, 5% w/w). The reaction was stirred at rt for 16 h under H_2 . After filtration on celite and purification on a silica gel column eluting with 20–60% EtOAc in CyH, the desired compound was obtained as a white solid (3.46 g, 14.7 mmol, 98%). $^1\text{H NMR}$ (500 MHz, CDCl_3): δ 9.27 (br s, 1H), 4.33 (q, $J = 7.1$ Hz, 2H), 3.22–3.13 (m, 1H), 2.68–2.63 (m, 2H), 2.52 (s, 3H), 1.87–1.79 (m, 4H), 1.37 (t, $J = 7.1$ Hz, 3H); $^{13}\text{C NMR}$ (126 MHz, CDCl_3): δ 200.1, 161.7, 138.6, 123.6, 134.3, 116.7, 60.5, 42.1, 25.4, 23.5, 21.9, 14.6, 14.0; HRMS (neg. ESI): calcd for $\text{C}_{13}\text{H}_{16}\text{NO}_3 \text{M} - \text{H}^-$, 234.1136; found, 234.1136; R_f : 0.47 (30% AcOEt in CyH).

4.12. 3-Methyl-4-oxo-2,4,5,6,7,8-hexahydrocyclohepta[c]-pyrrole-1-carboxylic Acid (31). To a solution of ethyl 3-methyl-4-oxo-2,4,5,6,7,8-hexahydrocyclohepta[c]pyrrole-1-carboxylate (1.15 g, 4.89 mmol, 1.0 equiv, 30) was dissolved in EtOH and aqueous 2 M NaOH (48.9 mL, 1:1). The mixture was heated at reflux overnight, cooled to 0°C , and neutralized until pH 1 using concentrated aqueous HCl (12 M). The precipitate was filtered and recrystallized using CHCl_3 to afford the desired product (723 mg, 3.49 mmol, 71%) as a white solid. $^1\text{H NMR}$ (500 MHz, $\text{DMSO}-d_6$): δ 12.44 (br s, 1H), 11.81 (br s, 1H), 3.15–3.11 (m, 2H), 2.55–2.50 (m, 2H), 2.36 (s, 3H), 1.75–1.65 (m, 4H); $^{13}\text{C NMR}$ (126 MHz, $\text{DMSO}-d_6$): δ 198.4, 162.3, 138.0, 133.0, 122.3, 116.6, 41.3, 24.8, 22.3, 21.2, 13.1; HRMS (pos. APCI) calcd for $\text{C}_{11}\text{H}_{14}\text{O}_3\text{N} [\text{M} + \text{H}]^+$, 208.0968; found, 208.0968; R_f : 0.63 (100% AcOEt + 2% AcOH).

4.13. 4-Methoxy-3-nitrobenzenesulfonyl Chloride (32). 4-Methoxybenzenesulfonyl chloride (15.0 g, 72.6 mmol, 1.0 equiv) was dissolved in H_2SO_4 (52 mL) at rt. Afterward, the solution was cooled to 0°C , and HNO_3 (5.2 mL, 0.11 mol, 1.5 equiv) was added dropwise. The mixture was stirred for 3.5 h at 0°C and then poured on ice, and the aqueous phase was extracted three times with Et₂O. The combined organic layers were washed with H_2O and brine, dried over Na_2SO_4 , and evaporated. The desired compound was obtained as a brown solid (13.8 g, 55.0 mmol, 76%). $^1\text{H NMR}$ (400 MHz, CDCl_3): δ 8.51 (d, $J = 2.5$ Hz, 1H), 8.21 (dd, $J = 9.0$ Hz, $J = 2.5$ Hz, 1H), 7.30 (d, $J = 9.0$ Hz, 1H), 4.11 (s, 3H); $^{13}\text{C NMR}$ (101 MHz, CDCl_3): δ 132.9, 129.7, 125.5, 114.9, 114.5, 57.7.

4.14. *N,N*-Diethyl-4-methoxy-3-nitrobenzenesulfonamide (33). To a solution of 4-methoxy-3-nitrobenzenesulfonyl chloride (4.53 g, 18.0 mmol, 1.0 equiv, 32) in CH_2Cl_2 (36 mL) at 0°C was added diethylamine (9.31 mL, 54.0 mmol, 3.0 equiv) dropwise. The solution was then stirred at rt for 16 h, washed with 1 M HCl, brine, dried over Na_2SO_4 , and evaporated. The residue was purified on a silica gel column eluting with 20–80% EtOAc in CyH to afford the desired product (5.15 g, 17.9 mmol, 99%) as a light yellow solid. $^1\text{H NMR}$ (500 MHz, CDCl_3): δ 8.23 (d, $J = 2.3$ Hz, 1H), 7.95 (dd, $J = 8.8, 2.3$ Hz, 1H), 7.19 (d, $J = 8.9$ Hz, 1H), 4.02 (s, 3H), 3.23 (q, $J = 7.1$ Hz, 4H), 1.13 (t, $J = 7.2$ Hz, 6H); $^{13}\text{C NMR}$ (126 MHz, CDCl_3): δ 155.4, 139.2, 132.8, 132.7, 124.8, 114.0, 57.1, 42.2, 14.2; HRMS (pos. ESI): calcd for $\text{C}_{11}\text{H}_{17}\text{N}_2\text{O}_5 \text{M} + \text{H}^+$, 289.0855; found, 289.0855; R_f : 0.38 (60% AcOEt in CyH).

4.15. 1-((4-Methoxy-3-nitrophenyl)sulfonyl)azepane (34). The compound was synthesized as reported for *N,N*-diethyl-4-methoxy-3-nitrobenzenesulfonamide to afford the desired compound (3.52 g, 11.2 mmol, 94%) as a light yellow solid. $^1\text{H NMR}$ (500 MHz, CDCl_3): δ 8.23 (d, $J = 2.3$ Hz, 1H), 7.95 (dd, $J = 8.8, 2.3$ Hz, 1H), 7.19 (d, $J = 8.9$ Hz, 1H), 4.03 (s, 3H), 3.32–3.19 (m, 4H), 1.76–1.68 (m, 4H), 1.63–1.53 (m, 4H); $^{13}\text{C NMR}$ (126 MHz, CDCl_3): δ 155.4, 139.3, 132.6, 132.0, 124.7, 113.9, 57.1, 48.4, 29.2, 26.9; HRMS (pos. ESI): calcd. for $\text{C}_{13}\text{H}_{19}\text{N}_2\text{O}_5 \text{M} + \text{H}^+$, 315.1009; found, 315.1009; R_f : 0.56 (60% AcOEt in CyH).

4.16. 4-((4-Methoxy-3-nitrophenyl)sulfonyl)morpholine (35). The compound was synthesized as reported for *N,N*-diethyl-4-methoxy-3-nitrobenzenesulfonamide to afford the desired compound (3.14 g, 10.4 mmol, 87%) as a light yellow solid. $^1\text{H NMR}$ (400 MHz, $\text{DMSO}-d_6$): δ 8.20 (d, $J = 2.3$ Hz, 1H), 8.00 (dd, $J = 8.9, 2.3$ Hz, 1H), 7.61 (d, $J = 9.0$ Hz, 1H), 4.04 (s, 3H), 3.68–3.60 (m, 4H), 2.96–2.88 (m, 4H); $^{13}\text{C NMR}$ (101 MHz, $\text{DMSO}-d_6$): δ 155.2, 138.9, 133.4, 126.3, 124.6, 115.4, 65.2, 57.4, 45.7; HRMS (pos. ESI): calcd for $\text{C}_{11}\text{H}_{14}\text{N}_2\text{O}_6\text{SNa} \text{M} + \text{Na}^+$, 325.0465; found, 325.0465; R_f : 0.35 (60% AcOEt in CyH).

4.17. 6-((4-Methoxy-3-nitrophenyl)sulfonyl)-2-oxa-6-azaspiro[3.3]heptane (36). To a solution of 4-methoxy-3-nitrobenzenesulfonyl chloride (0.50 g, 2.0 mmol, 1.2 equiv, 32) in CH_2Cl_2 (2 mL) were added 2-oxa-6-azaspiro[3.3]heptane oxalate (2:1, 0.24 g, 0.83 mmol, 0.5 equiv) and DIEA (0.85 mL, 0.65 g, 5.0 mmol, 3.0 equiv) at 0°C . The mixture was allowed to return to rt and stirred for 16 h. The mixture was washed with citric acid solution (5%, w/v), saturated Na_2CO_3 solution and brine; the combined organic layers were dried over Na_2SO_4 and evaporated. The residue was purified by reversed phase column chromatography eluting with 5–100% MeCN in H_2O to afford the desired product as a colorless solid (149 mg, 0.47 mmol, 29%). $^1\text{H NMR}$ (400 MHz, CDCl_3): δ 8.28 (d, $J = 2.3$ Hz, 1H), 7.99 (ddd, $J = 8.8, 2.3, 0.7$ Hz, 1H), 7.24 (d, $J = 8.8$ Hz, 1H), 4.67 (s, 4H), 4.06 (s, 3H), 3.98 (s, 4H); $^{13}\text{C NMR}$ (101 MHz, CDCl_3): δ 156.4, 133.8, 128.0, 126.1, 126.1, 114.1, 80.3, 59.8, 57.3, 37.8; HRMS (pos. ESI): calcd for $\text{C}_{12}\text{H}_{14}\text{O}_6\text{N}_2\text{NaS} [\text{M} + \text{Na}]^+$, 337.0465; found, 337.0460; R_f : 0.31 (66% AcOEt in PE).

4.18. 1-((4-Methoxy-3-nitrophenyl)sulfonyl)piperidine (37). Piperidine (10.6 mL, 107 mmol, 3.0 equiv) was added to a solution of 4-methoxy-3-nitrobenzenesulfonyl chloride (9.00 g, 35.8 mmol, 1.0 equiv) in CH_2Cl_2 (38 mL) at 0°C . The reaction mixture was allowed to return to rt and stirred for 16 h. The mixture was washed with citric acid solution (5%, w/v), saturated NaHCO_3 solution and brine, dried over Na_2SO_4 , and evaporated. The residue was purified on a silica gel column eluting with 30–50% EtOAc in PE to afford the desired product as a colorless solid (3.62 g, 12.0 mmol, 34%). $^1\text{H NMR}$ (300 MHz, CDCl_3): δ 8.54 (d, $J = 2.2$ Hz, 1H), 8.25 (dd, $J = 8.8, 2.3$ Hz, 1H), 7.56 (d, $J = 8.8$ Hz, 1H), 4.38 (s, 3H), 3.40–3.29 (m, 4H), 2.00 (p, $J = 5.8$ Hz, 4H), 1.85–1.73 (m, 2H); R_f : 0.48 (50% AcOEt in PE).

4.19. 1-((4-Methoxy-3-nitrophenyl)sulfonyl)-4-methylpiperazine (38). The compound was synthesized as reported for *N,N*-diethyl-4-methoxy-3-nitrobenzenesulfonamide to afford the desired compound (2.92 g, 9.26 mmol, 93%) as a light yellow solid. $^1\text{H NMR}$ (500 MHz, CDCl_3): δ 8.13–7.97 (m, 1H), 7.82–7.62 (m, 1H), 7.19 (d, $J = 8.9$ Hz, 1H), 3.93 (s, 3H), 2.98–2.79 (m, 4H), 2.37–2.28 (m, 4H), 2.13–2.07 (m, 3H); $^{13}\text{C NMR}$ (126 MHz, CDCl_3): δ 155.6, 138.8,

133.2, 127.1, 125.0, 114.1, 57.0, 53.6, 45.7, 45.3; HRMS (pos. ESI): calcd for $C_{12}H_{18}N_3O_3S$ M + H^+ , 316.0962; found, 316.0962; R_f : 0.17 (45% AcOEt in CyH + 0.1% NEt₃).

4.20. 3-Amino-*N,N*-diethyl-4-methoxybenzenesulfonamide (39). To a solution of 3-amino-*N,N*-diethyl-4-methoxybenzenesulfonamide (4.10 g, 14.2 mmol, 1.0 equiv, 33) in AcOEt/MeOH (50 mL) at rt under argon was added Pd/C (820 mg, 10% w/w). The solution was put under H₂ and stirred at rt for 16 h. The solution was filtered on celite and evaporated to afford the desired product (3.54 g, 13.7 mmol, 96%) as a light yellow solid. ¹H NMR (300 MHz, CDCl₃): δ 7.17 (dd, J = 8.4, 2.2 Hz, 1H), 7.10 (d, J = 2.2 Hz, 1H), 6.79 (d, J = 8.4 Hz, 1H), 3.99 (br s, 2H), 3.89 (s, 3H), 3.19 (q, J = 7.1 Hz, 5H), 1.11 (t, J = 7.1 Hz, 6H); ¹³C NMR (126 MHz, CDCl₃): δ 150.0, 136.7, 132.2, 118.0, 112.7, 109.6, 55.7, 42.1, 14.2; HRMS (pos. ESI): calcd for $C_{11}H_{19}N_2O_3S$ M + H^+ , 259.1111; found, 259.1111; R_f : 0.47 (33% AcOEt in CyH).

4.21. 3-Amino-*N,N*-diethyl-4-hydroxybenzenesulfonamide (40). The synthesis was done according to *J. Med. Chem.*, 2011, 54(9), 3241–3250 to afford the desired product as a yellow-brown solid (189 mg, 0.77 mmol, 20%). ¹H NMR (300 MHz, DMSO-*d*₆): δ 9.98 (br s, 1H), 7.00 (d, J = 2.2 Hz, 1H), 6.82 (dd, J = 8.2, 2.2 Hz, 1H), 6.75 (d, J = 8.2 Hz, 1H), 4.95 (br s, 2H), 3.07 (q, J = 7.1 Hz, 4H), 1.02 (t, J = 7.1 Hz, 6H); ¹³C NMR (101 MHz, DMSO-*d*₆): δ 147.5, 137.2, 129.8, 115.7, 113.5, 111.8, 41.6, 14.0.

4.22. 5-(Azepan-1-ylsulfonyl)-2-methoxyaniline (41). The compound was synthesized as reported for 3-amino-*N,N*-diethyl-4-methoxybenzenesulfonamide in MeOH/EtOAc (1:1, 50 mL) to afford the desired compound (1.72 g, 6.05 mmol, 95%) as a light yellow solid. ¹H NMR (400 MHz, DMSO-*d*₆): δ 8.86 (br s, 2H), 7.69 (d, J = 2.3 Hz, 1H), 7.51 (dd, J = 8.6, 2.4 Hz, 1H), 7.23 (dd, J = 8.7, 1.1 Hz, 1H), 3.92 (s, 3H), 3.25–3.13 (m, 4H), 1.73–1.42 (m, 8H); ¹³C NMR (101 MHz, DMSO-*d*₆): δ 153.2, 131.0, 127.0, 123.8, 118.8, 111.8, 56.3, 47.6, 28.4, 26.3; HRMS (pos. ESI): calcd. for $C_{13}H_{21}N_2O_3S$ M + H^+ , 285.1287; found, 285.1287; R_f : 0.48 (40% AcOEt in PE).

4.23. 2-Methoxy-5-(morpholin-1-ylsulfonyl)aniline (42). The compound was synthesized as reported for 3-amino-*N,N*-diethyl-4-methoxybenzenesulfonamide in MeOH/EtOAc (1:1, 50 mL) to afford the desired compound (1.89 g, 6.94 mmol, 91%) as a light yellow solid. ¹H NMR (500 MHz, DMSO-*d*₆): δ 7.04–6.94 (m, 2H), 6.93–6.78 (m, 1H), 3.84 (s, 3H), 5.25 (br s, 2H), 3.67–3.57 (m, 4H), 2.84–2.74 (m, 4H); ¹³C NMR (126 MHz, DMSO-*d*₆): δ 149.6, 138.3, 125.8, 116.2, 111.5, 109.9, 65.3, 55.6, 45.9; HRMS (pos. ESI): calcd. for $C_{11}H_{16}N_2O_4SNa$ M + Na^+ , 295.0723; found, 295.0723; R_f : 0.72 (80% AcOEt in CyH).

4.24. 5-((2-Oxa-6-azaspiro[3.3]heptan-6-yl)sulfonyl)-2-methoxyaniline (43). The compound was synthesized as reported for 2-methoxy-5-(piperidin-1-ylsulfonyl)aniline diluted in EtOAc/MeOH (2:1, 29 mL) to afford the desired compound (126 mg, 0.444 mmol, 93%) as a sticky colorless solid. ¹H NMR (500 MHz, CDCl₃): δ 7.20 (dd, J = 8.4, 2.2 Hz, 1H), 7.10 (d, J = 2.2 Hz, 1H), 6.87 (d, J = 8.4 Hz, 1H), 4.60 (s, 4H), 3.94 (s, 3H), 3.89 (s, 4H); ¹³C NMR (126 MHz, CDCl₃): 150.9, 136.9, 126.0, 119.5, 113.6, 109.8, 80.5, 59.6, 55.9, 37.6; HRMS (pos. ESI): calcd for $C_{12}H_{16}O_4N_2NaS$ [M + Na]⁺, 307.0723; found, 307.0724; R_f : 0.61 (3% MeOH in CH₂Cl₂).

4.25. 2-Methoxy-5-(piperidin-1-ylsulfonyl)aniline (44). Pd/C (150 mg, 10% w/w) was added to a solution of 1-((4-methoxy-3-nitrophenyl)sulfonyl)-piperidine (1.50 g, 4.99 mmol, 1.0 equiv, 37) in a mixture of EtOAc/MeOH (29 mL, 2:1) under argon. The reaction mixture was stirred overnight under H₂ (1 atm) at rt. The mixture was filtered over celite and afterward purified on a silica gel column eluting with 40% EtOAc in PE to obtain the desired product as a colorless solid (1.25 g, 4.62 mmol, 93%). ¹H NMR (500 MHz, CDCl₃): δ 7.12 (dd, J = 8.4, 2.2 Hz, 1H), 7.05 (d, J = 2.2 Hz, 1H), 6.83 (d, J = 8.4 Hz, 1H), 4.00 (br s, 2H), 3.91 (s, 3H), 3.00–2.86 (m, 4H), 1.62 (p, J = 6.0 Hz, 4H), 1.47–1.34 (m, 2H); ¹³C NMR (126 MHz, CDCl₃): δ 150.3, 136.7, 128.2, 118.8, 113.3, 109.7, 55.8, 47.1, 25.3, 23.7; HRMS (pos. ESI): calcd for $C_{12}H_{18}O_3N_2NaS$ [M + Na]⁺, 293.0930; found, 293.0930; R_f : 0.38 (6 7% AcOEt in PE).

4.26. 2-Methoxy-5-((4-methylpiperazin-1-yl)sulfonyl)aniline (45). The compound was synthesized as reported for 3-amino-*N,N*-diethyl-4-methoxybenzenesulfonamide in MeOH/EtOAc (1:1, 50 mL)

to afford the desired compound (1.66 g, 5.82 mmol, 92%) as a light yellow solid. The desired compound was directly used for the following step. HRMS (pos. ESI): calcd for $C_{12}H_{20}N_3O_3S$ M + H^+ , 286.1220; found, 286.1220.

4.27. Ethyl 2,3-Dimethyl-4-oxo-2,4,5,6,7,8-hexahydrocyclohepta[c]pyrrole-1-carboxylate (46). MeI (48 μ L, 109 mg, 0.779 mmol, 1.5 equiv) was added to a solution of ethyl 3-methyl-4-oxo-2,4,5,6,7,8-hexahydrocyclohepta[c]pyrrole-1-carboxylate (122 mg, 0.519 mmol, 1.0 equiv) and K₂CO₃ (142 mg, 1.38 mmol, 2.0 equiv) in DMF (2 mL). The reaction mixture was stirred at 50 °C overnight. The mixture was allowed to cool down before H₂O and EtOAc were added. The aqueous phase was extracted three times with EtOAc, the combined organic layers were dried over Na₂SO₄, evaporated, and purified by column chromatography (14–20% EtOAc in PE). The desired product was obtained as a yellow oil which crystallizes over time (109 mg, 0.436 mmol, 84%). ¹H NMR (500 MHz, CDCl₃): δ 1.38 (t, J = 7.1 Hz, 3H), 1.75–1.86 (m, 4H), 2.50 (s, 3H), 2.64 (m, 2H), 3.14 (m, 2H), 3.77 (s, 3H), 4.32 (q, J = 7.1 Hz, 2H). ¹³C NMR (126 MHz, CDCl₃): δ 11.7, 14.6, 22.0, 23.9, 25.4, 32.9, 42.0, 60.2, 119.2, 122.6, 134.7, 140.7, 162.2, 200.4. HRMS (pos. APCI): calcd for $C_{14}H_{20}NO_3$ [M + H]⁺, 250.1438; found, 250.1436.

4.28. 2,3-Dimethyl-4-oxo-2,4,5,6,7,8-hexahydrocyclohepta[c]pyrrole-1-carboxylic Acid (47). A solution of ethyl 2,3-dimethyl-4-oxo-2,4,5,6,7,8-hexahydrocyclohepta[c]pyrrole-1-carboxylate (100 mg, 0.401 mmol, 1.0 equiv) and NaOH (48 mg, 1.20 mmol, 3.0 equiv) in MeOH/H₂O (1.2 mL, 1:1) was stirred at 60 °C overnight. MeOH was evaporated, and the aqueous phase was acidified with conc. HCl to a pH of ~4. Afterward, the suspension was extracted three times with EA, dried over Na₂SO₄, and evaporated to obtain the title compound without further purification as a colorless solid, which decomposes via decarboxylation at rt to a red oil (73.4 mg, 0.332 mmol, 83%). ¹H NMR (500 MHz, acetone-*d*₆): δ 1.72–1.83 (m, 4H), 2.48 (s, 3H), 2.58 (m, 2H), 3.22 (m, 2H), 3.80 (s, 3H), 10.70 (br s, 1H). ¹³C NMR (126 MHz, acetone-*d*₆): δ 11.4, 22.4, 24.0, 26.1, 33.0, 42.3, 119.6, 123.0, 135.1, 141.2, 163.1, 199.3. HRMS (neg. ESI): calcd for $C_{12}H_{14}NO_3$ [M – H]⁺, 220.0979; found, 220.0980.

4.29. *N*,3-Dimethyl-4-oxo-2,4,5,6,7,8-hexahydrocyclohepta[c]pyrrole-1-carboxamide (6). Ghosez's reagent (437 μ L, 0.796 mmol, 1.1 equiv) was added to a solution of 3-methyl-4-oxo-2,4,5,6,7,8-hexahydrocyclohepta[c]pyrrole-1-carboxylic acid (150 mg, 0.724 mmol, 1.0 equiv, 31) in dry CH₂Cl₂ (4.8 mL) at rt. The reaction mixture was stirred for 30 min before methylamine in THF (2 M, 1.1 mL, 2.17 mmol, 3.0 equiv) was added. The reaction was stirred overnight at rt. The solvent was evaporated, and the residue was purified by column chromatography eluting with 2–6% MeOH in CH₂Cl₂. The desired compound was obtained as an orange solid (102 mg, 0.463 mmol, 64%). ¹H NMR (400 MHz, CDCl₃): δ 9.52 (br s, 1H), 5.64 (br s, 1H), 3.01 (s, 3H), 2.97–2.91 (m, 2H), 2.70–2.63 (m, 2H), 2.50 (d, J = 0.6 Hz, 3H), 1.93–1.83 (m, 4H); ¹³C NMR (101 MHz, CDCl₃): δ 199.6, 162.7, 137.2, 126.2, 123.1, 120.6, 42.0, 26.6, 26.0, 24.9, 13.8; HRMS (pos. APCI): calcd for $C_{12}H_{17}O_2N_2$ [M + H]⁺, 221.1285; found, 221.1278; R_f : 0.37 (6% MeOH in CH₂Cl₂).

4.30. *N*-(5-(*N,N*-Diethylsulfamoyl)-2-hydroxyphenyl)-3-methyl-4-oxo-2,4,5,6,7,8-hexahydrocyclohepta[c]pyrrole-1-carboxamide (7). To a solution of 3-methyl-4-oxo-2,4,5,6,7,8-hexahydrocyclohepta[c]pyrrole-1-carboxylic acid (50 mg, 0.24 mmol, 1.0 equiv, 31) in DMF (2 mL) was added NEt₃ (67 μ L, 0.48 mmol, 2.0 equiv). The resulting mixture was stirred at rt for 10 min, after which time was added CDI (30 mg, 0.27 mmol, 1.1 equiv). The mixture was stirred at rt for 1 h, after which time was added 3-amino-*N,N*-diethyl-4-hydroxybenzenesulfonamide (65 mg, 0.48 mmol, 1.1 equiv, 40). The mixture was stirred at 65 °C for 16 h. The mixture was purified on a silica gel column eluting with 40–100% EtOAc in PE to obtain the desired product as a white solid (9 mg, 0.02 mmol, 9%). ¹H NMR (400 MHz, DMSO-*d*₆): δ 11.98 (br s, 1H), 11.08 (br s, 1H), 8.75 (br s, 1H), 8.44 (d, J = 2.3 Hz, 1H), 7.39 (dd, J = 8.5, 2.4 Hz, 1H), 7.05 (d, J = 8.5 Hz, 1H), 3.21–3.08 (m, 6H), 2.62–2.52 (m, 2H), 2.41 (s, 3H), 1.82–1.70 (m, 4H), 1.05 (t, J = 7.1 Hz, 6H); ¹³C NMR (101 MHz, DMSO-*d*₆): δ 198.3, 159.4, 150.9, 137.2, 130.3, 129.7, 126.6, 123.4, 122.3,

120.0, 119.7, 115.0, 41.7, 41.3, 25.1, 22.9, 21.3, 14.0, 13.1; HRMS (pos. ESI): calcd for $C_{12}H_{17}O_3N_2$ [$M + H$] $^+$, 456.15636; found, 456.15636.

4.31. *N*-(5-(*N,N*-Diethylsulfamoyl)-2-methoxyphenyl)-3-methyl-4-oxo-2,4,5,6,7,8-hexahydrocyclohepta[c]pyrrole-1-carboxamide (8). To a solution of 3-methyl-4-oxo-2,4,5,6,7,8-hexahydrocyclohepta[c]pyrrole-1-carboxylic acid (100 mg, 0.48 mmol, 1.00 equiv, **31**) and 3-amino-*N,N*-diethyl-4-methoxybenzenesulfonamide (156 mg, 0.60 mmol, 1.25 equiv, **39**) in dry DMF (1.9 mL) at 0 °C were added DIEA (0.42 mL, 2.41 mmol, 5.00 equiv) and HCTU (250 mg, 0.60 mmol, 1.25 equiv). The reaction was allowed to warm at rt. After 4 h, the mixture was heated at 100 °C for 16 h. Then, DMF was evaporated. Water was added, and the aqueous phase was extracted three times with EtOAc. The combined organics were washed with 1 M HCl, saturated Na_2CO_3 , brine, and dried over Na_2SO_4 . Purification on a silica gel column eluting with 20–100% EtOAc in CyH to afford the desired product (139 mg, 0.31 mmol, 64%) as a light yellow solid. 1H NMR (400 MHz, $CDCl_3$): δ 10.13 (br s, 1H), 8.84 (d, J = 2.3 Hz, 1H), 8.22 (s, 1H), 7.52 (dd, J = 8.5, 2.3 Hz, 1H), 6.93 (d, J = 8.7 Hz, 1H), 3.98 (s, 3H), 3.22 (q, J = 7.1 Hz, 4H), 3.15–3.06 (m, 2H), 2.72–2.62 (m, 2H), 2.49 (d, J = 0.5 Hz, 3H), 2.00–1.80 (m, 4H), 1.11 (t, J = 7.2 Hz, 6H); ^{13}C NMR (101 MHz, $CDCl_3$): δ 199.5, 159.8, 150.6, 138.6, 132.8, 128.1, 127.9, 123.5, 123.2, 120.7, 118.1, 109.6, 56.5, 42.2, 41.9, 25.8, 24.5, 21.8, 14.3, 13.7; HRMS (pos. ESI): calcd for $C_{22}H_{29}N_3O_5SNa$ [$M + Na$] $^+$, 470.1720; found, 470.1720; R_f : 0.57 (66% AcOEt in CyH).

4.32. *N*-(5-(Azepan-1-ylsulfonyl)-2-methoxyphenyl)-3-methyl-4-oxo-2,4,5,6,7,8-hexahydrocyclohepta[c]pyrrole-1-carboxamide (9). The compound was synthesized as reported for *N*-(5-(*N,N*-diethylsulfamoyl)-2-methoxyphenyl)-3-methyl-4-oxo-2,4,5,6,7,8-hexahydrocyclohepta[c]pyrrole-1-carboxamide (**8**) to afford the desired compound (167 mg, 0.35 mmol, 73%) as a light yellow solid. 1H NMR (400 MHz, $CDCl_3$): δ 10.07 (br s, 1H), 8.83 (d, J = 2.3 Hz, 1H), 8.23 (s, 1H), 7.51 (dd, J = 8.6, 2.3 Hz, 1H), 6.94 (d, J = 8.6 Hz, 1H), 3.99 (s, 3H), 3.31–3.23 (m, 4H), 3.12–3.07 (m, 2H), 2.72–2.63 (m, 2H), 2.49 (d, J = 0.5 Hz, 3H), 1.99–1.82 (m, 4H), 1.68 (dt, J = 10.9, 4.7, 2.4 Hz, 4H), 1.61–1.52 (m, 4H); ^{13}C NMR (101 MHz, $CDCl_3$): δ 199.5, 159.8, 150.6, 138.6, 132.1, 128.1, 127.9, 123.5, 123.1, 120.8, 117.9, 109.6, 56.5, 48.4, 41.9, 29.2, 27.0, 25.8, 24.5, 21.8, 13.7; HRMS (pos. ESI): calcd for $C_{24}H_{31}N_3O_5SNa$ [$M + Na$] $^+$, 496.1877; found, 496.1877; R_f : 0.40 (66% AcOEt in CyH).

4.33. *N*-(2-Methoxy-5-(morpholin-1-ylsulfonyl)phenyl)-3-methyl-4-oxo-2,4,5,6,7,8-hexahydrocyclohepta[c]pyrrole-1-carboxamide (10). The compound was synthesized as reported for *N*-(5-(*N,N*-diethylsulfamoyl)-2-methoxyphenyl)-3-methyl-4-oxo-2,4,5,6,7,8-hexahydrocyclohepta[c]pyrrole-1-carboxamide (**8**) to afford the desired compound (84 mg, 0.18 mmol, 38%) as a light yellow solid. 1H NMR (400 MHz, $CDCl_3$): δ 9.90 (br s, 1H), 8.83 (d, J = 2.3 Hz, 1H), 8.25 (s, 1H), 7.48 (dd, J = 8.6, 2.3 Hz, 1H), 7.01 (d, J = 8.7 Hz, 1H), 4.02 (s, 3H), 3.77–3.65 (m, 4H), 3.13–3.07 (m, 2H), 3.05–2.98 (m, 4H), 2.71–2.66 (m, 2H), 2.50 (s, 3H), 2.01–1.85 (m, 4H); ^{13}C NMR (101 MHz, $CDCl_3$): δ 199.5, 159.8, 151.1, 138.7, 128.3, 127.8, 127.7, 124.0, 123.6, 120.7, 118.9, 109.8, 66.2, 56.6, 46.2, 41.9, 25.9, 24.7, 21.8, 13.8; HRMS (pos. ESI): calcd for $C_{22}H_{27}N_3O_6SNa$ [$M + Na$] $^+$, 484.1513; found, 484.1513; R_f : 0.19 (66% AcOEt in CyH).

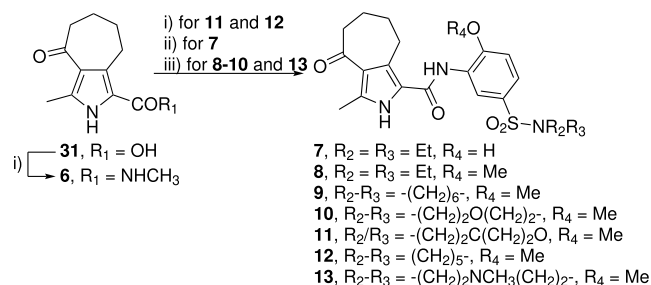
4.34. *N*-(5-(2-Oxa-6-azaspiro[3.3]heptan-6-yl)sulfonyl)-2-methoxyphenyl)-3-methyl-4-oxo-2,4,5,6,7,8-hexahydrocyclohepta[c]pyrrole-1-carboxamide (11). The compound was synthesized as reported for 2-methoxy-5-(piperidin-1-ylsulfonyl)phenyl 3-methyl-4-oxo-2,4,5,6,7,8-hexahydrocyclohepta[c]pyrrole-1-carboxylate (**12**) in CH_2Cl_2 (1.8 mL) to afford the desired compound (25 mg, 0.05 mmol, 29%) as a colorless solid. 1H NMR (500 MHz, $CDCl_3$): δ 10.00 (s, 1H), 8.86 (d, J = 2.3 Hz, 1H), 8.23 (s, 1H), 7.55 (dd, J = 8.6, 2.3 Hz, 1H), 7.03 (d, J = 8.7 Hz, 1H), 4.58 (s, 4H), 4.03 (s, 3H), 3.94 (s, 4H), 3.13–3.08 (m, 2H), 2.72–2.66 (m, 2H), 2.51 (s, 3H), 1.99–1.87 (m, 4H); ^{13}C NMR (126 MHz, $CDCl_3$): δ 199.6, 159.8, 151.5, 138.8, 128.3, 128.0, 126.7, 124.5, 123.6, 120.6, 119.4, 109.8, 80.4, 59.8, 56.7, 41.9, 37.6, 25.9, 24.6, 21.8, 13.8; HRMS (pos. ESI): calcd for $C_{23}H_{27}O_6N_3SNa$ [$M + Na$] $^+$, 496.1513; found, 496.1511.

4.35. 2-Methoxy-5-(piperidin-1-ylsulfonyl)phenyl 3-methyl-4-oxo-2,4,5,6,7,8-hexahydrocyclohepta[c]pyrrole-1-carboxy-

late (12). To a solution of 3-methyl-4-oxo-2,4,5,6,7,8-hexahydrocyclohepta[c]pyrrole-1-carboxylic acid (50 mg, 0.24 mmol, 1.0 equiv, **31**) in dry CH_2Cl_2 (2.4 mL) was added dropwise 1-chloro-*N,N*,2-trimethyl-1-propenylamine (36 μ L, 0.27 mmol, 1.1 equiv). The reaction was stirred for 30 min at rt. Subsequently, 1-((4-methoxy-3-nitrophenyl)sulfonyl)piperidine (98 mg, 0.36 mmol, 1.5 equiv, **44**) and DIEA (47 μ L, 0.48 mmol, 2.0 equiv) were added to the reaction mixture. After stirring overnight at rt, the solvent was evaporated. The residue was purified by reversed phase chromatography eluting with 5–95% MeCN in H_2O to afford the desired compound as a colorless solid (75 mg, 0.16 mmol, 68%). 1H NMR (400 MHz, $CDCl_3$): δ 9.66 (br s, 1H), 8.81 (d, J = 2.3 Hz, 1H), 8.22 (s, 1H), 7.50 (dd, J = 8.6, 2.3 Hz, 1H), 6.99 (d, J = 8.6 Hz, 1H), 4.01 (s, 3H), 3.15–3.08 (m, 2H), 3.06–3.01 (m, 4H), 2.73–2.67 (m, 2H), 2.51 (s, 3H), 2.01–1.86 (m, 4H), 1.66–1.62 (m, 4H), 1.47–1.35 (m, 2H); ^{13}C NMR (101 MHz, $CDCl_3$): δ 199.5, 159.7, 150.8, 138.4, 129.1, 128.1, 127.6, 123.9, 123.7, 120.7, 118.9, 109.6, 56.6, 47.1, 42.0, 25.9, 25.3, 24.7, 23.7, 21.9, 13.8; HRMS (pos. ESI): calcd for $C_{23}H_{29}O_5N_3NaS$ [$M + Na$] $^+$, 482.1720; found, 482.1723; R_f : 0.21 (50% AcOEt in CyH).

4.36. *N*-(2-Methoxy-5-((4-methylpiperazin-1-yl)sulfonyl)phenyl)-3-methyl-4-oxo-2,4,5,6,7,8-hexahydrocyclohepta[c]pyrrole-1-carboxamide (13). The compound was synthesized as reported for *N*-(5-(*N,N*-diethylsulfamoyl)-2-methoxyphenyl)-3-methyl-4-oxo-2,4,5,6,7,8-hexahydrocyclohepta[c]pyrrole-1-carboxamide (**8**) to afford the desired compound (94 mg, 0.20 mmol, 41%) as a light yellow solid. 1H NMR (400 MHz, $CDCl_3$): δ 9.98 (br s, 1H), 8.83 (d, J = 2.3 Hz, 1H), 8.23 (s, 1H), 7.47 (dd, J = 8.6, 2.3 Hz, 1H), 6.98 (d, J = 8.7 Hz, 1H), 4.00 (s, 3H), 3.14–2.99 (m, 6H), 2.73–2.62 (m, 2H), 2.49 (d, J = 0.4 Hz, 3H), 2.45 (t, J = 5.0 Hz, 4H), 2.24 (s, 3H), 2.00–1.81 (m, 4H); ^{13}C NMR (101 MHz, $CDCl_3$): δ 199.5, 159.7, 151.0, 138.6, 128.3, 127.9, 127.7, 123.9, 123.6, 120.8, 118.8, 109.7, 56.6, 54.2, 46.1, 45.8, 41.9, 25.9, 24.6, 21.8, 13.8; HRMS (pos. ESI): calcd for $C_{23}H_{31}N_4O_5S$ [$M + H$] $^+$, 475.2010; found, 475.2010; R_f : 0.36 (12% MeOH in CH_2Cl_2 + 0.1% NEt_3) (Scheme 3).

Scheme 3. Synthesis of Final Compounds 6–13^a.

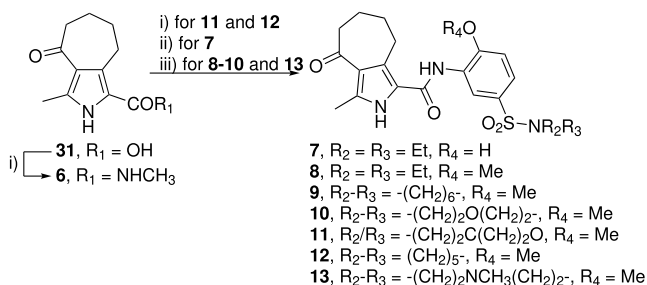


^aReagents and conditions: (i) Ghose's reagent, CH_2Cl_2 , rt, then $MeNH_2$ in THF or **43–44**, DIEA, rt, 29–68%; (ii) CDI, **40**, NEt_3 , rt to 65 °C, 9%; (iii) HCTU, **39**, **41–42** or **45**, DIEA, DMF, 0–100 °C, 38–73%.

4.37. *N*-(2-Methoxy-5-(piperidin-1-ylsulfonyl)phenyl)-2,3-dimethyl-4-oxo-2,4,5,6,7,8-hexahydrocyclohepta[c]pyrrole-1-carboxamide (14). Ghose's reagent (14 μ L, 14 mg, 0.11 mmol, 1.2 equiv) was added to a solution of 2,3-dimethyl-4-oxo-2,4,5,6,7,8-hexahydrocyclohepta[c]pyrrole-1-carboxylic acid (32 mg, 0.14 mmol, 1.0 equiv) in dry CH_2Cl_2 (0.9 mL). The reaction mixture was stirred for 30 min before 2-methoxy-5-(piperidin-1-ylsulfonyl)aniline (37 mg, 0.14 mmol, 1.5 equiv) and DIEA (46 μ L, 35 mg, 0.27 mmol, 2% 1% 3.0 equiv) were added. The reaction was stirred overnight at rt. The solvents were evaporated, and the residue was purified by reversed phase column chromatography (MeCN/ H_2O). The desired compound was obtained as a colorless oil (25 mg, 53 μ mol, 59%). 1H NMR (500 MHz, $CDCl_3$): δ 1.44 (td, J = 7.2, 6.2, 4.4 Hz, 2H), 1.66 (p, J = 5.8 Hz, 4H), 1.88 (p, J = 2.9 Hz, 4H), 2.53 (s, 3H), 2.64–2.70 (m, 2H), 2.97–3.03 (m, 2H), 3.04–3.10 (m, 4H), 3.73 (s, 3H), 3.99 (s, 3H), 7.00 (d, J = 8.6 Hz, 1H), 7.54 (dd, J = 8.6, 2.3 Hz, 1H), 8.04 (s, 1H), 8.87 (d, J = 2.2 Hz, 1H); ^{13}C NMR (126 MHz, $CDCl_3$): δ 11.5, 19.0, 21.8, 23.7,

23.9, 25.4, 25.8, 32.1, 41.8, 47.2, 56.5, 109.7, 118.9, 121.8, 124.2, 127.6, 128.1, 129.2, 140.0, 150.9, 160.1, 199.8; HRMS (neg. ESI): calcd for $C_{24}H_{30}N_3O_3S$ [$M - H$]⁻, 472.1912; found, 472.1911 (Scheme 4).

Scheme 4. Synthesis of Final Compounds 14^a



^aReagents and conditions: (i) MeI, K_2CO_3 , DMF, 50 °C, 84%; (ii) LiOH·H₂O, THF/MeOH/H₂O, rt, 83%; (iii) Ghosez reagent, CH_2Cl_2 , rt, then **47**, DIEA, CH_2Cl_2 , rt, 59%.

4.38. Model Building. The model (Figure 6) of **11** bound to the BD of BRD9 was created with the help of SeeSAR.⁴³ For this purpose, an alignment of the binding pockets of BRD9 (PDB ID 4UIW) and BRD4(1) in complex with **11** was carried out. Then, **11** was transferred into the binding pocket of BRD9 and binding poses were generated.

4.39. Isothermal Titration Calorimetry. ITC experiments were performed with a Microcal VP-ITC microcalorimeter (Malvern Instruments, Herrenberg, Germany) at 25 °C (unless otherwise stated) using ligand concentrations between 10 and 60 μM in the sample cell and BRD4(1) concentrations between 100 and 600 μM in the injection syringe. Concentrations were determined gravimetrically (ligands) and by the native absorption coefficient at 280 nm wavelength (protein). The protein concentration was additionally cross-validated by titration against a gravimetrically determined amount of **2**. The processing of the raw data was carried out using NITPIC⁴⁴ (automatic baseline correction and spike integration). The fitting of the data was done with the help of ITCsy⁴⁵ using a binary binding model. Concentration errors were automatically corrected by ITCsy. For the evaluation of the generated fits, the P-level at 95 and 99% for ΔH and ΔG were additionally calculated.

4.40. Protein Preparation, Crystallization, and Structure Determination. BRD4(1) was produced as described previously.¹³ Co-crystals were obtained in the Index HT Screen (Hampton Research) or the PEGsmear Screen⁴⁶ at 10 mg/mL and a ligand concentration of 2 mM from a 100 mM stock solution in DMSO added directly to the protein prior to crystallization. Data were collected at 100 K. Data collection took place at the PXI and PXIII beamlines at the Swiss Light Source at $\lambda = 1.000$ Å with an EIGER 16M detector and a Pilatus 2M-F, respectively. Datasets were indexed with XDS⁴⁷ and scaled and merged with Aimless,^{48,49} as implemented in the CCP4 suite.⁵⁰ Molecular replacement was done with Phaser⁵¹ as implemented in PHENIX⁵² using a previously published structure as search model (BRD4(1) PDB ID code 4LYI¹³). Reciprocal space model refinement using Phenix.refine^{53–55} from the PHENIX suite, REFMAC5^{56,57} from the CCP4 suite and autoBUSTER⁵⁸ was combined with real space refinement in COOT⁵⁹ in an iterative way. Ligands were modelled into 2Fo-Fc electron density maps by hand. Final structure validation was done with PROCHECK/SFCHECK⁶⁰ or MolProbity.⁶¹

4.41. Cell Culture Viability Assay. SK-MEL-5 cells (RRID: CVCL_0527) were obtained from CLS Cell Lines Service GmbH and cultivated in supplemented EMEM. MCF-7 cells (RRID: CVCL_0031) were kindly provided by Prof. Süss, University Freiburg, and cultivated in supplemented RPMI1640. HeLa cells (RRID: CVCL_0030) were kindly provided by Prof. Aktories, University Freiburg, and cultivated in supplemented DMEM. HL-60 cells (RRID: CVCL_0002) were kindly provided by Prof. Lübbert, University Hospital Freiburg, and cultivated in supplemented RPMI1640. The cell culture media DMEM and RPMI1640 (both PAN Biotech) were

supplemented with 10% (v/v) FCS (PAN Biotech), 2 mM L-glutamine (PAN Biotech), and 1% (v/v) Penicillin/Streptomycin (PAN Biotech). EMEM media (CLS, Cell Lines Service) was supplemented with 10% (v/v) FCS and 1% (v/v) Penicillin/Streptomycin. SK-MEL-5 (3000 cell well⁻¹), MCF-7 (3000 cell well⁻¹), and HeLa (2000 cell well⁻¹) cells were seeded in 96-well plates and allowed to grow overnight. Compounds were dissolved in DMSO, diluted in cell culture media, and added in triplicates to the cells to a final DMSO concentration of 0.5%. HL-60 cells were diluted to 5 $\times 10^4$ cells mL⁻¹ and mixed with in DMSO dissolved compounds to a final DMSO concentration of 0.5% and seeded in 96-well plates in triplicates. After 72 h incubation in a 5% CO₂ atmosphere at 37 °C, the CellTiter 96S Aqueous Non-Radioactive Cell Proliferation Assay from Promega was performed according to the manufacturer's instructions. Assay plates were measured at 49 nm on a POLARstar Optima microplate reader (BMG Labtech, Ortenberg, Germany). All mean values from triplicates were blank-subtracted and related to the normalized vehicle control to 100% viability of cells. The calculations for the combination index were done as described by Chou and Talalay.³⁵

■ ASSOCIATED CONTENT

Supporting Information

The Supporting Information is available free of charge at <https://pubs.acs.org/doi/10.1021/acs.jmedchem.0c00478>.

Abbreviations, molecular strings (SMILES), schemes, NMR spectra, X-ray data collection and model refinement statistics, NCI results with Z Scores for all GI values, ITC thermograms, DiscoverX results, dose response curves for GI₅₀ determination, combination experiments for **15** ((+)-JQ1) with **18** (LP99) and model coordinates for compound **11** bound to BRD9 (PDF)

SMILE strings of all shown molecules and corresponding affinities (CSV)

PDB coordinates file of the modeled complex of BRD9 (PDB ID 4UIW) with **11** (PDB)

Accession Codes

Authors will release the atomic coordinates and experimental data upon article publication. Atomic coordinates and structure factors were deposited in the Protein Data Bank: BRD4(1)-**6** PDB ID 6RWJ, BRD4(1)-**7** PDB ID 6SB8, BRD4(1)-**8** PDB ID 6S4B, BRD4(1)-**9** PDB ID 6S6K, BRD4(1)-**10** PDB ID 6SA2, BRD4(1)-**11** PDB ID 6SAH, BRD4(1)-**12** PDB ID 6SAJ, BRD4(1)-**13** PDB ID 6SA3.

■ AUTHOR INFORMATION

Corresponding Author

Stefan Günther – Institut für Pharmazeutische Wissenschaften, Albert-Ludwigs-Universität Freiburg, D-79104 Freiburg, Germany; orcid.org/0000-0003-3744-189X; Phone: +49-(0)761-203-4871; Email: stefan.guenther@pharmazie.uni-freiburg.de; Fax: +49-(0)761-203-97769

Authors

Martin Hügler – Institut für Pharmazeutische Wissenschaften and Institut für Biochemie, Albert-Ludwigs-Universität Freiburg, D-79104 Freiburg, Germany

Pierre Regenass – Institut für Organische Chemie, Albert-Ludwigs-Universität Freiburg, D-79104 Freiburg, Germany

Robin Warstat – Institut für Organische Chemie, Albert-Ludwigs-Universität Freiburg, D-79104 Freiburg, Germany

Mirjam Hau – Institut für Pharmazeutische Wissenschaften and CIBSS/Centre for Integrative Biological Signalling Studies, Albert-Ludwigs-Universität Freiburg, D-79104 Freiburg, Germany

Karin Schmidtkunz – Institut für Pharmazeutische Wissenschaften, Albert-Ludwigs-Universität Freiburg, D-79104 Freiburg, Germany

Xavier Lucas – Institut für Pharmazeutische Wissenschaften, Albert-Ludwigs-Universität Freiburg, D-79104 Freiburg, Germany; orcid.org/0000-0003-0887-3976

Daniel Wohlwend – Institut für Biochemie, Albert-Ludwigs-Universität Freiburg, D-79104 Freiburg, Germany; orcid.org/0000-0001-6782-5822

Oliver Einsle – Institut für Biochemie, Albert-Ludwigs-Universität Freiburg, D-79104 Freiburg, Germany; orcid.org/0000-0001-8722-2893

Manfred Jung – Institut für Pharmazeutische Wissenschaften, Albert-Ludwigs-Universität Freiburg, D-79104 Freiburg, Germany; orcid.org/0000-0002-6361-7716

Bernhard Breit – Institut für Organische Chemie, Albert-Ludwigs-Universität Freiburg, D-79104 Freiburg, Germany; orcid.org/0000-0002-2514-3898

Complete contact information is available at:

<https://pubs.acs.org/10.1021/acs.jmedchem.0c00478>

Author Contributions

M.H. and P.R. contributed equally. The manuscript was written through contributions of all authors. All authors have given approval to the final version of the manuscript. M.H. purified BRD4(1), did ITC, crystallization, and X-ray data collection, solved the crystal structures, designed 6–14, and prepared the manuscript. P.R. and R.W. designed and carried out the synthesis of 6–14 and helped drafting the manuscript. M.H. determined the GI50s. K.S. determined CIs. X.L. designed 6. D.W. carried out X-ray data collection and helped drafting the manuscript. O.E., M.J., B.B., and S.G. helped designing the study and drafting the manuscript.

Funding

This study was supported by the German Research Foundation (DFG): GU1225/3-1, WO2012/1-1, Germany's Excellence Strategy (CIBSS—EXC-2189—Project ID 390939984), CRC 992 "Medical Epigenetics".

Notes

The authors declare no competing financial interest.

ACKNOWLEDGMENTS

The authors thank the staff of the Swiss Light Source (SLS) beamlines X06SA and X06DA for their excellent technical support.

ABBREVIATIONS

¹H, proton NMR spectroscopy; ¹³C, carbon NMR spectroscopy; AcOH, acetic acid; APCI, atmospheric pressure chemical ionization; *n*-BuLi, *n*-butyllithium; Calcd, calculated; CDCl₃, deuterated chloroform; CDI, carbonyldiimidazole; CHCl₃, chloroform; CH₂Cl₂, dichloromethane; CI, combination index; CyH, cyclohexane; DIEA, *N,N*-diisopropylethylamine; Et₂NH, diethylamine; EtOAc, ethyl acetate; EtOH, ethanol; H₂, dihydrogen; H₂O, water; HCl, hydrochloric acid; HCTU, O-(1*H*-6-chlorobenzotriazole-1-yl)-1,1,3,3-tetramethyluronium hexafluorophosphate; HR-MS, high resolution mass spectrometry; LC50, lethal concentration, 50%; pH, potential of hydrogen; Na₂CO₃, sodium carbonate; NaHCO₃, sodium hydrogen carbonate; NaNO₂, sodium nitrite; NaOH, sodium hydroxide; Na₂SO₄, sodium sulfate; NEt₃, triethylamine; NBS, *N*-bromosuccinimide; NH₄Cl, ammonium chloride; NH₄OAc,

ammonium acetate; Pd/C, palladium on charcoal; PE, petroleum ether; PhMe, toluene; PTSA, *p*-toluenesulfonic acid; PPh₃, triphenylphosphine; TGI, total growth inhibition; Zn, zinc

REFERENCES

- (1) Goldberg, A. D.; Allis, C. D.; Bernstein, E. Epigenetics: a landscape takes shape. *Cell* **2007**, *128*, 635–638.
- (2) Muller, S.; Filippakopoulos, P.; Knapp, S. Bromodomains as therapeutic targets. *Expert Rev. Mol. Med.* **2011**, *13*, No. e29.
- (3) Filippakopoulos, P.; Knapp, S. The bromodomain interaction module. *FEBS Lett.* **2012**, *586*, 2692–2704.
- (4) Filippakopoulos, P.; Picaud, S.; Mangos, M.; Keates, T.; Lambert, J.-P.; Barsyte-Lovejoy, D.; Felletar, I.; Volkmer, R.; Müller, S.; Pawson, T.; Gingras, A.-C.; Arrowsmith, C. H.; Knapp, S. Histone recognition and large-scale structural analysis of the human bromodomain family. *Cell* **2012**, *149*, 214–231.
- (5) Shi, J.; Vakoc, C. R. The mechanisms behind the therapeutic activity of BET bromodomain inhibition. *Mol. Cell* **2014**, *54*, 728–736.
- (6) Naka, Y.; Ichiyanagi, Y.; Haga, K.; Hosoya, S. Thienodiazepine Compound. Japan Patent JPH0228181A; Yoshitomi Pharmaceutical Industries, Ltd., 1990.
- (7) Marmorstein, R.; Berger, S. L. Structure and function of bromodomains in chromatin-regulating complexes. *Gene* **2001**, *272*, 1–9.
- (8) Filippakopoulos, P.; Qi, J.; Picaud, S.; Shen, Y.; Smith, W. B.; Fedorov, O.; Morse, E. M.; Keates, T.; Hickman, T. T.; Felletar, I.; Philpott, M.; Munro, S.; McKeown, M. R.; Wang, Y.; Christie, A. L.; West, N.; Cameron, M. J.; Schwartz, B.; Heightman, T. D.; La Thangue, N.; French, C. A.; Wiest, O.; Kung, A. L.; Knapp, S.; Bradner, J. E. Selective inhibition of BET bromodomains. *Nature* **2010**, *468*, 1067–1073.
- (9) Nicodeme, E.; Jeffrey, K. L.; Schaefer, U.; Beinke, S.; Dewell, S.; Chung, C.-W.; Chandwani, R.; Marazzi, I.; Wilson, P.; Coste, H.; White, J.; Kirilovsky, J.; Rice, C. M.; Lora, J. M.; Prinjha, R. K.; Lee, K.; Tarakhovskiy, A. Suppression of inflammation by a synthetic histone mimic. *Nature* **2010**, *468*, 1119–1123.
- (10) Romero, F. A.; Taylor, A. M.; Crawford, T. D.; Tsui, V.; Côté, A.; Magnuson, S. Disrupting acetyl-lysine recognition: progress in the development of bromodomain inhibitors. *J. Med. Chem.* **2016**, *59*, 1271–1298.
- (11) Meng, S.; Zhang, L.; Tang, Y.; Tu, Q.; Zheng, L.; Yu, L.; Murray, D.; Cheng, J.; Kim, S. H.; Zhou, X.; Chen, J. BET inhibitor JQ1 blocks inflammation and bone destruction. *J. Dent. Res.* **2014**, *93*, 657–662.
- (12) Anand, P.; Brown, J. D.; Lin, C. Y.; Qi, J.; Zhang, R.; Artero, P. C.; Alaiti, M. A.; Bullard, J.; Alazem, K.; Margulies, K. B.; Cappola, T. P.; Lemieux, M.; Plutzky, J.; Bradner, J. E.; Haldar, S. M. BET bromodomains mediate transcriptional pause release in heart failure. *Cell* **2013**, *154*, 569–582.
- (13) Lucas, X.; Wohlwend, D.; Hügle, M.; Schmidtkunz, K.; Gerhardt, S.; Schüle, R.; Jung, M.; Einsle, O.; Günther, S. 4-Acyl pyrroles: mimicking acetylated lysines in histone code reading. *Angew. Chem.* **2013**, *52*, 14055–14059.
- (14) Hügle, M.; Lucas, X.; Weitzel, G.; Ostrovskiy, D.; Breit, B.; Gerhardt, S.; Einsle, O.; Günther, S.; Wohlwend, D. 4-Acyl pyrrole derivatives yield novel vectors for designing inhibitors of the acetyl-lysine recognition site of BRD4(1). *J. Med. Chem.* **2016**, *59*, 1518–1530.
- (15) Doroshow, D. B.; Eder, J. P.; LoRusso, P. M. BET inhibitors: a novel epigenetic approach. *Ann. Oncol.* **2017**, *28*, 1776–1787.
- (16) Fong, C. Y.; Gilan, O.; Lam, E. Y. N.; Rubin, A. F.; Ftouni, S.; Tyler, D.; Stanley, K.; Sinha, D.; Yeh, P.; Morison, J.; Giotopoulos, G.; Lugo, D.; Jeffrey, P.; Lee, S. C.-W.; Carpenter, C.; Gregory, R.; Ramsay, R. G.; Lane, S. W.; Abdel-Wahab, O.; Kouzarides, T.; Johnstone, R. W.; Dawson, S.-J.; Huntly, B. J. P.; Prinjha, R. K.; Papenfuss, A. T.; Dawson, M. A. BET inhibitor resistance emerges from leukaemia stem cells. *Nature* **2015**, *525*, 538–542.

- (17) Braun, T.; Gardin, C. Investigational BET bromodomain protein inhibitors in early stage clinical trials for acute myelogenous leukemia (AML). *Expert Opin. Invest. Drugs* **2017**, *26*, 803–811.
- (18) Pérez-Salvia, M.; Esteller, M. Bromodomain inhibitors and cancer therapy: From structures to applications. *Epigenetics* **2017**, *12*, 323–339.
- (19) Andrieu, G.; Belkina, A. C.; Denis, G. V. Clinical trials for BET inhibitors run ahead of the science. *Drug Discov. Today* **2016**, *19*, 45–50.
- (20) Hügle, M.; Lucas, X.; Ostrovskiy, D.; Regenass, P.; Gerhardt, S.; Einsle, O.; Hau, M.; Jung, M.; Breit, B.; Günther, S.; Wohlwend, D. Beyond the BET family: targeting CBP/p300 with 4-acyl pyrroles. *Angew. Chem., Int. Ed.* **2017**, *56*, 12476–12480.
- (21) Martin, L. J.; Koegl, M.; Bader, G.; Cockcroft, X.-L.; Fedorov, O.; Fiegen, D.; Gerstberger, T.; Hofmann, M. H.; Hohmann, A. F.; Kessler, D.; Knapp, S.; Knesl, P.; Kornigg, S.; Müller, S.; Nar, H.; Rogers, C.; Rumpel, K.; Schaaf, O.; Steurer, S.; Tallant, C.; Vakoc, C. R.; Zeeb, M.; Zoephel, A.; Pearson, M.; Boehmelt, G.; McConnell, D. Structure-based design of an in vivo active selective BRD9 inhibitor. *J. Med. Chem.* **2016**, *59*, 4462–4475.
- (22) Takeda and SGC, TP-472 a BRD9/7 Probe. <http://www.thesgc.org/chemical-probes/TP-472>, (accessed Oct 9, 2020).
- (23) Theodoulou, N. H.; Bamborough, P.; Bannister, A. J.; Becher, I.; Bit, R. A.; Che, K. H.; Chung, C.-w.; Dittmann, A.; Drewes, G.; Drewry, D. H.; Gordon, L.; Grandi, P.; Leveridge, M.; Lindon, M.; Michon, A.-M.; Molnar, J.; Robson, S. C.; Tomkinson, N. C. O.; Kouzarides, T.; Prinjha, R. K.; Humphreys, P. G. Discovery of I-BRD9, a selective cell active chemical probe for bromodomain containing protein 9 inhibition. *J. Med. Chem.* **2016**, *59*, 1425–1439.
- (24) Crawford, T. D.; Vartanian, S.; Côté, A.; Bellon, S.; Duplessis, M.; Flynn, E. M.; Hewitt, M.; Huang, H.-R.; Kiefer, J. R.; Murray, J.; Nasveschuk, C. G.; Pardo, E.; Romero, F. A.; Sandy, P.; Tang, Y.; Taylor, A. M.; Tsui, V.; Wang, J.; Wang, S.; Zawadzke, L.; Albrecht, B. K.; Magnuson, S. R.; Cochran, A. G.; Stokoe, D. Inhibition of bromodomain-containing protein 9 for the prevention of epigenetically-defined drug resistance. *Bioorg. Med. Chem. Lett.* **2017**, *27*, 3534–3541.
- (25) Hohmann, A. F.; Martin, L. J.; Minder, J. L.; Roe, J.-S.; Shi, J.; Steurer, S.; Bader, G.; McConnell, D.; Pearson, M.; Gerstberger, T.; Gottschamel, T.; Thompson, D.; Suzuki, Y.; Koegl, M.; Vakoc, C. R. Sensitivity and engineered resistance of myeloid leukemia cells to BRD9 inhibition. *Nat. Chem. Biol.* **2016**, *12*, 672–679.
- (26) Bevil, S. M.; Olivares-Quintero, J. F.; Sciaky, N.; Golitz, B. T.; Singh, D.; Beltran, A. S.; Rashid, N. U.; Stuhlmiller, T. J.; Hale, A.; Moorman, N. J.; Santos, C. M.; Angus, S. P.; Zawistowski, J. S.; Johnson, G. L. GSK2801, a BAZ2/BRD9 bromodomain inhibitor, synergizes with BET inhibitors to induce apoptosis in triple-negative breast Cancer. *Mol. Cancer Res.* **2019**, *17*, 1503–1518.
- (27) Ferriz, J. M.; Vinsova, J. Prodrug design of phenolic drugs. *Curr. Pharm. Des.* **2010**, *16*, 2033–2052.
- (28) Wuitschik, G.; Carreira, E. M.; Wagner, B.; Fischer, H.; Parrilla, I.; Schuler, F.; Rogers-Evans, M.; Müller, K. Oxetanes in drug discovery: structural and synthetic insights. *J. Med. Chem.* **2010**, *53*, 3227–3246.
- (29) *Comprehensive Medicinal Chemistry*, 3rd ed.; Martinez, A., Gil, C., Eds.; Elsevier: Amsterdam, the Netherlands and Oxford, United Kingdom, 2017.
- (30) Zheng, Y.; Tice, C. M.; Singh, S. B. The use of spirocyclic scaffolds in drug discovery. *Bioorg. Med. Chem. Lett.* **2014**, *24*, 3673–3682.
- (31) Quinn, E. Integrated Solution for targeting epigenetics using human cell model Systems and novel in vitro assays <https://www.discoverx.com/CMSPages/GetAmazonFile.aspx?path=%5Cdiscoverx%5Cfiles%5C7f%5C7ff245f-a5ff-415d-aa79-63ce3bfb96c3.pdf#=a95de5d658112be617573e0cf751bc0c674d8e168b5ff35a9ab410ebb1lad560>, (accessed Oct 9, 2020), 2010.
- (32) Clark, P. G. K.; Vieira, L. C. C.; Tallant, C.; Fedorov, O.; Singleton, D. C.; Rogers, C. M.; Monteiro, O. P.; Bennett, J. M.; Baronio, R.; Müller, S.; Daniels, D. L.; Méndez, J.; Knapp, S.; Brennan, P. E.; Dixon, D. J. LP99: discovery and synthesis of the first selective BRD7/9 bromodomain inhibitor. *Angew. Chem.* **2015**, *54*, 6217–6221.
- (33) Picaud, S.; Fedorov, O.; Thanasopoulou, A.; Leonards, K.; Jones, K.; Meier, J.; Olzscha, H.; Monteiro, O.; Martin, S.; Philpott, M.; Tumber, A.; Filippakopoulos, P.; Yapp, C.; Wells, C.; Che, K. H.; Bannister, A.; Robson, S.; Kumar, U.; Parr, N.; Lee, K.; Lugo, D.; Jeffrey, P.; Taylor, S.; Vecellio, M. L.; Bountra, C.; Brennan, P. E.; O'Mahony, A.; Velichko, S.; Müller, S.; Hay, D.; Daniels, D. L.; Urh, M.; La Thangue, N. B.; Kouzarides, T.; Prinjha, R.; Schwaller, J.; Knapp, S. Generation of a selective small molecule inhibitor of the CBP/p300 bromodomain for leukemia therapy. *Cancer Res.* **2015**, *75*, 5106–5119.
- (34) Shoemaker, R. H. The NCI60 human tumour cell line anticancer drug screen. *Nat. Rev. Cancer* **2006**, *6*, 813–823.
- (35) Chou, T.-C.; Talalay, P. Quantitative analysis of dose-effect relationships: the combined effects of multiple drugs or enzyme inhibitors. *Adv. Enzym. Regul.* **1984**, *22*, 27–55.
- (36) Bijnisdorp, I. V.; Giovannetti, E.; Peters, G. J. *Methods in Molecular Biology*; Humana Press, 2011; pp 421–434.
- (37) Waring, M. J.; Chen, H.; Rabow, A. A.; Walker, G.; Bobby, R.; Boiko, S.; Bradbury, R. H.; Callis, R.; Clark, E.; Dale, I.; Daniels, D. L.; Dulak, A.; Flavell, L.; Holdgate, G.; Jowitt, T. A.; Kikhney, A.; McAlister, M.; Méndez, J.; Ogg, D.; Patel, J.; Petteruti, P.; Robb, G. R.; Robers, M. B.; Saif, S.; Stratton, N.; Svergun, D. I.; Wang, W.; Whittaker, D.; Wilson, D. M.; Yao, Y. Potent and selective bivalent inhibitors of BET bromodomains. *Nat. Chem. Biol.* **2016**, *12*, 1097–1104.
- (38) Bedford, M. T.; Clarke, S. G. Protein arginine methylation in mammals: who, what, and why. *Mol. Cell* **2009**, *33*, 1–13.
- (39) Gadd, M. S.; Testa, A.; Lucas, X.; Chan, K.-H.; Chen, W.; Lamont, D. J.; Zengerle, M.; Ciulli, A. Structural basis of PROTAC cooperative recognition for selective protein degradation. *Nat. Chem. Biol.* **2017**, *13*, 514–521.
- (40) Kim, H. N.; Nichols, C.; Jiang, E. J.; Abdel-Azim, N.; Coba, A.; Durden, D. L.; Kim, Y.-M. Dual targeting of PI3Kdelta and BRD4 sensitizes acute lymphoblastic leukemia to chemotherapy. *Blood* **2018**, *132*, 1420.
- (41) Divakaran, A.; Talluri, S. K.; Ayoub, A. M.; Mishra, N. K.; Cui, H.; Widen, J. C.; Berndt, N.; Zhu, J.-Y.; Carlson, A. S.; Topczewski, J. J.; Schonbrunn, E. K.; Harki, D. A.; Pomerantz, W. C. K. Molecular basis for the N-terminal bromodomain-and-extra-terminal-family selectivity of a dual kinase-bromodomain inhibitor. *J. Med. Chem.* **2018**, *61*, 9316–9334.
- (42) Liu, S.; Yosief, H. O.; Dai, L.; Huang, H.; Dhawan, G.; Zhang, X.; Muthengi, A. M.; Roberts, J.; Buckley, D. L.; Perry, J. A.; Wu, L.; Bradner, J. E.; Qi, J.; Zhang, W. Structure-guided design and development of potent and selective dual bromodomain 4 (BRD4)/polo-like kinase 1 (PLK1) inhibitors. *J. Med. Chem.* **2018**, *61*, 7785–7795.
- (43) BioSolveIT GmbH, Sankt Augustin, Germany, SeeSAR version 9.1, 2019.
- (44) Keller, S.; Vargas, C.; Zhao, H.; Piszczek, G.; Brautigam, C. A.; Schuck, P. High-precision isothermal titration calorimetry with automated peak-shape analysis. *Anal. Chem.* **2012**, *84*, 5066–5073.
- (45) Brautigam, C. A.; Zhao, H.; Vargas, C.; Keller, S.; Schuck, P. Integration and global analysis of isothermal titration calorimetry data for studying macromolecular interactions. *Nat. Protoc.* **2016**, *11*, 882–894.
- (46) Chaikuad, A.; Knapp, S.; von Delft, F. Defined PEG smears as an alternative approach to enhance the search for crystallization conditions and crystal-quality improvement in reduced screens. *Acta Crystallogr., Sect. D: Biol. Crystallogr.* **2015**, *71*, 1627–1639.
- (47) Kabsch, W. Xds. *Acta Crystallogr., Sect. D: Biol. Crystallogr.* **2010**, *66*, 125–132.
- (48) Evans, P. R. An introduction to data reduction: space-group determination, scaling and intensity statistics. *Acta Crystallogr., Sect. D: Biol. Crystallogr.* **2011**, *67*, 282–292.
- (49) Evans, P. Scaling and assessment of data quality. *Acta Crystallogr., Sect. D: Biol. Crystallogr.* **2006**, *62*, 72–82.

- (50) Collaborative Computational Project Number 4. The CCP4 suite: programs for protein crystallography. *Acta Crystallogr., Sect. D: Biol. Crystallogr.* **1994**, *50*, 760–763.
- (51) McCoy, A. J.; Grosse-Kunstleve, R. W.; Adams, P. D.; Winn, M. D.; Storoni, L. C.; Read, R. J. Phaser crystallographic software. *J. Appl. Crystallogr.* **2007**, *40*, 658–674.
- (52) Adams, P. D.; Afonine, P. V.; Bunkóczi, G.; Chen, V. B.; Davis, I. W.; Echols, N.; Headd, J. J.; Hung, L.-W.; Kapral, G. J.; Grosse-Kunstleve, R. W.; McCoy, A. J.; Moriarty, N. W.; Oeffner, R.; Read, R. J.; Richardson, D. C.; Richardson, J. S.; Terwilliger, T. C.; Zwart, P. H. PHENIX: a comprehensive python-based system for macromolecular structure solution. *Acta Crystallogr., Sect. D: Biol. Crystallogr.* **2010**, *66*, 213–221.
- (53) Afonine, P. V.; Grosse-Kunstleve, R. W.; Adams, P. D.; Urzhumtsev, A. Bulk-solvent and overall scaling revisited: faster calculations, improved results. *Acta Crystallogr., Sect. D: Biol. Crystallogr.* **2013**, *69*, 625–634.
- (54) Afonine, P. V.; Grosse-Kunstleve, R. W.; Echols, N.; Headd, J. J.; Moriarty, N. W.; Mustyakimov, M.; Terwilliger, T. C.; Urzhumtsev, A.; Zwart, P. H.; Adams, P. D. Towards automated crystallographic structure refinement with phenix.refine. *Acta Crystallogr., Sect. D: Biol. Crystallogr.* **2012**, *68*, 352–367.
- (55) Afonine, P. V.; Grosse-Kunstleve, R. W.; Urzhumtsev, A.; Adams, P. D. Automatic multiple-zone rigid-body refinement with a large convergence radius. *J. Appl. Crystallogr.* **2009**, *42*, 607–615.
- (56) Murshudov, G. N.; Vagin, A. A.; Dodson, E. J. Refinement of macromolecular structures by the maximum-likelihood method. *Acta Crystallogr., Sect. D: Biol. Crystallogr.* **1997**, *53*, 240–255.
- (57) Murshudov, G. N.; Skubák, P.; Lebedev, A. A.; Pannu, N. S.; Steiner, R. A.; Nicholls, R. A.; Winn, M. D.; Long, F.; Vagin, A. A. REFMAC5 for the refinement of macromolecular crystal structures. *Acta Crystallogr., Sect. D: Biol. Crystallogr.* **2011**, *67*, 355–367.
- (58) Bricogne, G.; Blanc, E.; Brandl, M.; Flensburg, C.; Keller, P.; Paciorek, W. *BUSTER*, 2016.
- (59) Emsley, P.; Cowtan, K. Coot: model-building tools for molecular graphics. *Acta Crystallogr., Sect. D: Biol. Crystallogr.* **2004**, *60*, 2126–2132.
- (60) Vaguine, A. A.; Richelle, J.; Wodak, S. J. SFCHECK: a unified set of procedures for evaluating the quality of macromolecular structure-factor data and their agreement with the atomic model. *Acta Crystallogr., Sect. D: Biol. Crystallogr.* **1999**, *55*, 191–205.
- (61) Chen, V. B.; Arendall, W. B.; Headd, J. J.; Keedy, D. A.; Immormino, R. M.; Kapral, G. J.; Murray, L. W.; Richardson, J. S.; Richardson, D. C. MolProbity: all-atom structure validation for macromolecular crystallography. *Acta Crystallogr., Sect. D: Biol. Crystallogr.* **2010**, *66*, 12–21.